forests

MDPI

Article

Mapping the Urban Atmospheric Carbon Stock by LiDAR and WorldView-3 Data

MD Abdul Mueed Choudhury [1,*], Ernesto Marcheggiani [1,2,*], Andrea Galli [1], Giuseppe Modica [3] and Ben Somers [2]

[1] Department of Agricultural, Food, and Environmental Sciences, Marche Polytechnic University, 60131 Ancona, Italy; a.galli@staff.univpm.it
[2] Division of Forest, Nature, and Landscape, Department of Earth and Environmental Sciences, KU Leuven, 3001 Leuven, Belgium; ben.somers@kuleuven.be
[3] Dipartimento di Agraria, Università degli Studi Mediterranea di Reggio Calabria, Località Feodi Vito, 89122 Reggio Calabria, Italy; giuseppe.modica@unirc.it
* Correspondence: m.choudhury@pm.univpm.it (M.A.M.C.); e.marcheggiani@staff.univpm.it (E.M.)

Abstract: Currently, the worsening impacts of urbanizations have been impelled to the importance of monitoring and management of existing urban trees, securing sustainable use of the available green spaces. Urban tree species identification and evaluation of their roles in atmospheric Carbon Stock (CS) are still among the prime concerns for city planners regarding initiating a convenient and easily adaptive urban green planning and management system. A detailed methodology on the urban tree carbon stock calibration and mapping was conducted in the urban area of Brussels, Belgium. A comparative analysis of the mapping outcomes was assessed to define the convenience and efficiency of two different remote sensing data sources, Light Detection and Ranging (LiDAR) and WorldView-3 (WV-3), in a unique urban area. The mapping results were validated against field estimated carbon stocks. At the initial stage, dominant tree species were identified and classified using the high-resolution WorldView3 image, leading to the final carbon stock mapping based on the dominant species. An object-based image analysis approach was employed to attain an overall accuracy (OA) of 71% during the classification of the dominant species. The field estimations of carbon stock for each plot were done utilizing an allometric model based on the field tree dendrometric data. Later based on the correlation among the field data and the variables (i.e., Normalized Difference Vegetation Index, NDVI and Crown Height Model, CHM) extracted from the available remote sensing data, the carbon stock mapping and validation had been done in a GIS environment. The calibrated NDVI and CHM had been used to compute possible carbon stock in either case of the WV-3 image and LiDAR data, respectively. A comparative discussion has been introduced to bring out the issues, especially for the developing countries, where WV-3 data could be a better solution over the hardly available LiDAR data. This study could assist city planners in understanding and deciding the applicability of remote sensing data sources based on their availability and the level of expediency, ensuring a sustainable urban green management system.

Keywords: urban trees; Geospatial Object-Based Image Analysis (GEOBIA); Carbon Stock (CS) mapping; allometric model; WorldView-3 (WV-3) imagery; aerial Light Detection and Ranging (LiDAR) data

Citation: Choudhury, M.A.M.; Marcheggiani, E.; Galli, A.; Modica, G.; Somers, B. Mapping the Urban Atmospheric Carbon Stock by LiDAR and WorldView-3 Data. *Forests* **2021**, *12*, 692. https://doi.org/10.3390/f12060692

Academic Editor: Mark Vanderwel

Received: 25 April 2021
Accepted: 26 May 2021
Published: 28 May 2021

1. Introduction

To date, rapid urbanization intensely poses the need for greener landscapes in many urban areas worldwide. Green spaces allow maximizing urban resilience and livability and to positively respond to climate change effects. While cities are striving for more green space, more than half of the earth's population is already living in cities, and by 2050, 66% will be city dwellers [1]. Overexploitation of environmental resources for the huge population is indeed increasing the vulnerability of the urban dwellers to natural hazards.

To keep pace with rapid urbanization, efficient urban green planning could be nothing but a time being and an expeditious solution. Conservation and expansion of existing urban vegetation based on their structural and functional roles in an urban atmosphere are some of the most effective factors of green urban planning. Thus, various approaches based on advanced technologies have been implemented to assess the contributions of urban trees, especially evaluation of their roles in atmospheric Carbon Stock (CS) is being increasingly acknowledged [2,3]. Trees in city streets and parks are now being recognized as a key tool against impacts caused by the increased rate of atmospheric carbon dioxide (CO_2) concentrations [4–7], since they sequester atmospheric carbon during the whole growth process and at the same time delay the adverse effects of climate change contributing to the accumulation of carbon in the soil [8–10]. Studies found that the total yearly reduction in carbon emission can be up to 18 kg/tree in urban areas [11–13], which clearly brings out the importance of planting trees along with having an efficient tree management policy, especially in a complex city environment. Trees directly impact atmospheric CO_2 fixation through photosynthesis, but in urban areas, the process is quite fitful due to tree health issues. As it is well known that the well-grown trees store far more carbon than the poorly grown ones, in urban areas, it is a huge challenge to maintain and preserve mature trees and well-managed urban forests that also include tree plantations and replacements. Therefore an efficient and timewise monitoring approach is essential to introduce an adequate urban tree management system [14,15]. In addition an effective monitoring system could be ensured utilizing an accurate and convenient species-based CS mapping approach. Most of the CS calibration and predictive models are based on the estimation of Above Ground Biomass (AGB) production [13,16–20], which is considered to be primarily responsible for the atmospheric CS [10,21–23]. In this study, the AGB was estimated based on the tree allometric information (i.e., Height (H), Diameter at Breast Height (DBH)) collected during the field surveys.

Currently, remote sensing-based mapping has been availed as an influential approach in monitoring functional and structural urban tree features to policymakers [24–31]. In fact, spatially extracted information on tree species and habitats over large areas are significant in understanding species' roles, such as in providing ecosystem functions and services [32–35]. Over the last few decades, remote sensing-based classification of tree species has been widely utilized either in the case of mapping specific species-based ecosystem services (ES) outcomes (i.e., [36]), or growth and yield models and, etc. (e.g., [33,37,38]). Remote sensing approaches, especially hyperspectral imagery, have significantly upgraded the tree classification outcomes either in single trees or mixed populations [33,39–43]. The utilization of very high spatial resolution multispectral satellite imagery (e.g., 1-m IKONOS, 0.6-m QuickBird) and aerial photos/digital imagery has been rapidly increased, especially in spatial mapping [44–47]. As a matter of fact, recently, with the advancements of remote sensing technologies, a diversified type of very high resolution remotely sensed images (such as WorldView-3, WV-3) are commercially available, certainly introducing a wave of opportunities for the accurate mapping of urban trees at a significant level [31,33,48–52]. Moreover, in the case of this study, a high-resolution WV-3 image has been successfully utilized to classify the dominant tree species in Brussels, which has been found useful for further CS mapping as it was earlier in the case of Sassuolo [36].

Additionally, there are also many convincing applications of Light Detection and Ranging (LiDAR) based calibration of the tree CS utilizing the individual tree metrics (i.e., [53–61]). On the other hand, much less evidence is available in the CS calibration of the urban trees utilizing only the multispectral satellite data [11]. In the case of urban areas, tree species mapping is still a considerable challenge due to having spatially heterogeneous land cover types from isolated trees to the dense forest, high tree species diversity along with heavily and regularly managed trees, as well as the interruptions by buildings and their shadows [7,62–66]. Considering these facts, Geospatial Object-Based Image Analysis (GEOBIA) has been utilized in this study to classify the dominant tree species.

However, it is yet a crucial concern to dig out the most convenient and compatible ways to map and predict the urban tree CS in a specific urban area. A method could be considered convenient in various ways, such as its application, time consumption, and execution expenses. Even LiDAR application is the most acceptable and widely reliable, it is still expensive and hardly cost-effective for the more significant part of the world. Therefore, it would be a timely consideration to analyse the utilization of multispectral satellite data (i.e., Sentinel-2, WorldView-2/3/4) regarding CS computation possibilities of the trees in an urban area. A remote sensing-based biomass assessment has been employed in many studies [10,67–69] to obtain forest information over a large area at a reasonable cost with acceptable accuracy and minimal effort [70]. It is also evident that the method of determining relationships between field estimations and remote sensing data-derived variables and then extrapolating these relationships over large areas is very useful [10,71–78]. Here, the main goal of this study was to map the urban tree CS based on field measurements and the application of remote sensing tools considering the following:

- A comparative analysis of the application of two different remote sensing data sources (i.e., LiDAR and WV-3 image data) regarding CS mapping in the case of dominant urban tree species;
- To recommend an approach in the case of CS mapping for policymakers involving urban green management.

In a word, this study has been done to provide a fundamental tool considering urban CS mapping, which is one of the most critical issues for sustainable urban green management systems and their policymakers.

2. Materials and Methods

2.1. Dataset

2.1.1. Field Data

The study area, covering an area of around 49 km^2 in the eastern part of the capital region in Belgium (Figure 1), was selected considering the availability of airborne LiDAR.

As the main goal of this study was to identify only the dominant urban tree species, all other non-dominant vegetations have been excluded during sampling. The sample plots were randomly selected, covering only the streets of the whole study area. Since in the parks most of the cases of tree crowns were overlapped and or completely overshadowed by the other species. That is why overcrowded tree populations were excluded to avoid misinterpretations of the species dominance information, during the final CS mapping. During field data collection, 75 plots (yellow dots in Figure 2) of 100 m^2 (10 m $\times$ 10 m) each were selected throughout the study area following the well-known Simple Random Sampling (SRS) approach [79–82]. Only the areas with tree species dominance (i.e., woody or tall perennial plants) have been considered, excluding the ornamental herbs, shrubs, or grassland areas. The sample plots were also used during the training and validation of the tree species for GEOBIA classification. Among the 75 plots, 20 plots (red square boxes in Figure 2) were considered for the CS mapping and validation. The Diameter at Breast Height (DBH) was measured for each tree in the plot. The height (H) of trees was measured utilizing the hypsometer Nikon Forestry 550, a laser rangefinder with angle compensation technology optimized for forestry use [83], and a field computer was used to mark the plots on QGIS. Field data (H, DBH) were collected in the summer of 2019.

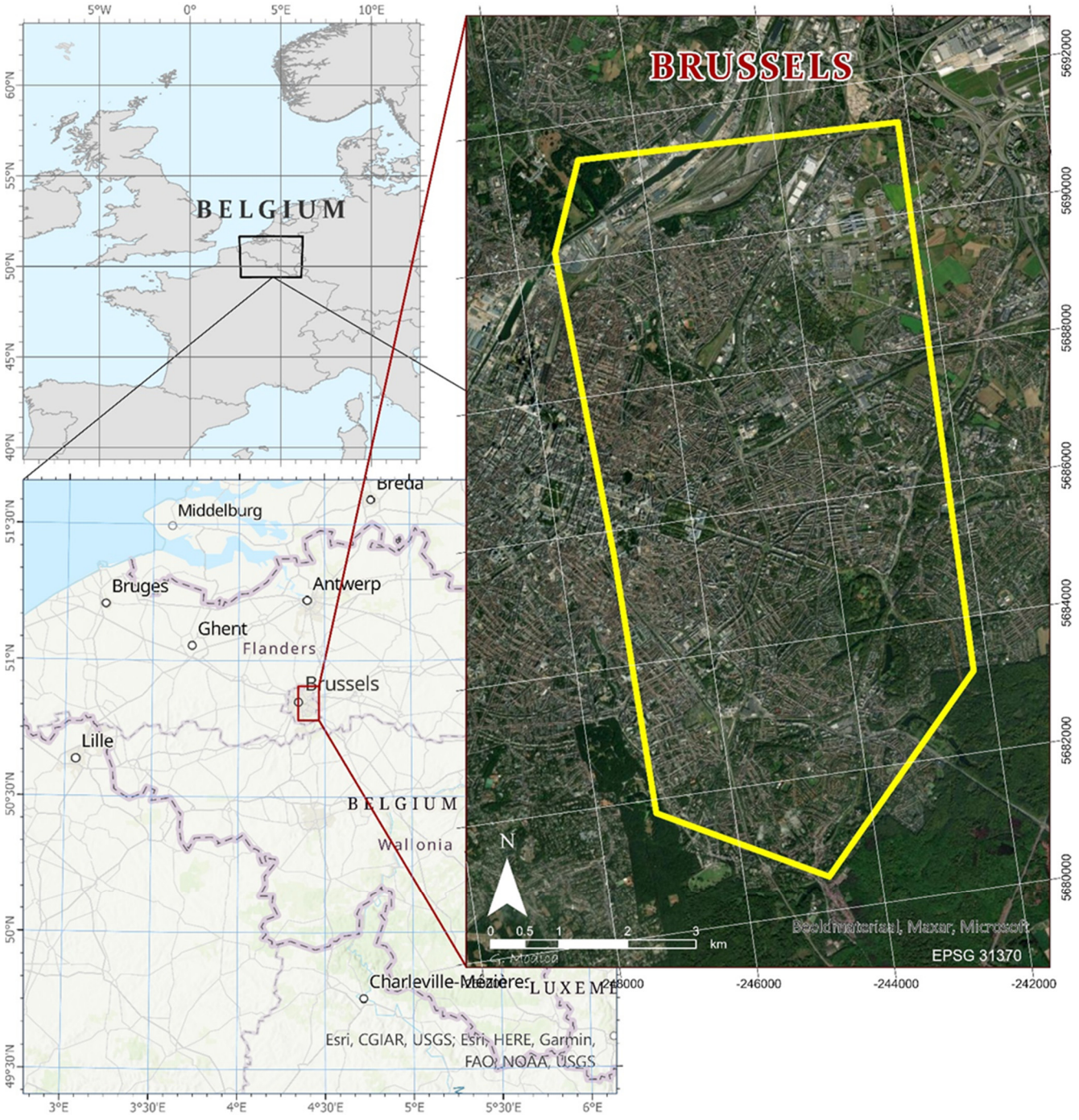

Figure 1. The study area at the eastern part of the urban area in Brussels (Belgium).

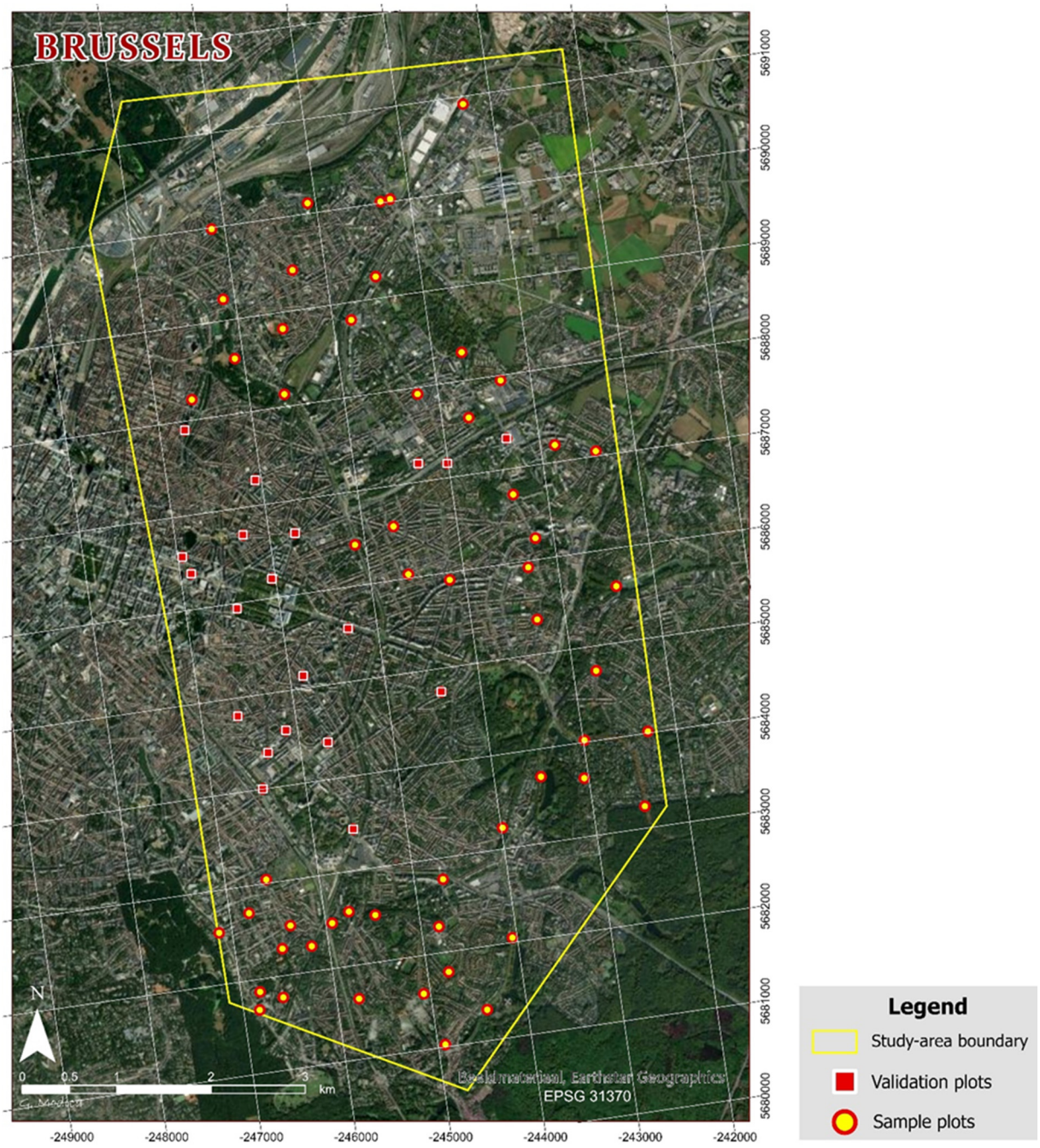

Figure 2. The map shows the distribution of sample and validation point to the estimation of Carbon Stocks (CS) superimposed over the WorldView-3 (WV-3) image data of the study area in Brussels.

2.1.2. Remote Sensing Data

The airborne LiDAR dataset had been collected in Summer 2015 by Aerodata Surveys Nederland BV [84]. The Crown Height Model (CHM), i.e., the height of objects obtained through the difference between the digital surface model (DSM) and the digital terrain model (DTM), was produced at a spatial resolution of 0.25 m using the LAStools software [84].

The WV3 image data for this study was acquired on 17 April 2017 (Figure 2), which provides one panchromatic band of 0.3 m and eight multispectral bands at 1.2 m spatial resolution (Table 1). The available WV-3 image data have been pan-sharpened at the initial stage. Pan-sharpening is the process of merging high-resolution panchromatic and multispectral imagery where the outcome is an image that has the high spectral resolu-

tion of the multispectral image and also the high spatial resolution of the panchromatic image [85–87].

Table 1. The eight multispectral bands of the WorldView-3 (WV-3) satellite imagery.

Bands	Wavelength [nm]
Coastal band	400–450
Blue band	450–510
Green band	510–580
Yellow band	585–625
Red band	630–690
Red edge band	705–715
Near-Infrared (NIR)1 band	770–895
Near-Infrared (NIR)2 band	860–1040

The pan-sharpen process was conducted using the hyperspectral colour sharpening (HCS) algorithm that combines the high-resolution panchromatic data with lower resolution multispectral data and specifically implemented for the WV imagery [88]. The cubic convolution resampling technique was chosen to resample the multispectral image to the high-resolution image using a 4 × 4 pixel moving window. The pan image and the multispectral image have been separately orthorectified using the DSM downloaded from the GeoPunt portal [89] and the available LiDAR data. All the steps were conducted in an ERDAS Imagine environment [90]. Later, the required shapefiles (for classification in Ecognition) were educed from the UrbIS database (UrbIS P& B and UrbIS-Adm), a general GIS database of the Brussels region [91].

2.2. Methodology

2.2.1. Geospatial Object-Based Image Analysis (GEOBIA) Classification

Tree species classification based on spectral properties is quite a matter of contention due to the high intra-class spectral heterogeneity and/or inter-class spectral similarities [7,44,64–66]. The traditional pixel-based procedures, which classify each object only based on a distinct spectral signature (ignoring other spatial/contextual information) [48,92,93], are hardly capable of reaching an acceptable accuracy [94,95]. In our study, GEOBIA was applied, which is already approved as an efficient technique in the case of high-resolution image classifications [48,85,92,96–99]. Instead of the single pixels, the GEOBIA approach typically works on: (i) Segmenting a remote sensing image into spectral similarities (i.e., segments or objects), and (ii) Evaluating the spectral, spatial, and/or context features of these segments for image classification [48,63,94,100,101]. As a result of segmentation, this approach can consider the textual and contextual information along with the spectral information during the classification [48,94,102–104]. Therefore GEOBIA classification outcomes are more acceptable than those based on the existing traditional pixel-based approach [102,105–111].

The Trimble eCognition Developer® 9 platform (Trimble, Munich, Germany) [112] was utilized to classify the dominant tree species in Brussels (Figure 3). At the initial stage, the chessboard segmentation has been introduced to initiate the GEOBIA classification approach. Then the primary classification was done utilizing the available shapefile from the Urbis database [91]. After that, the contrast split segmentation algorithm was implied to define the green and non-green areas with higher accuracy. This approach is based on the Normalized Difference Vegetation Index (NDVI) layer, where the 'contrast split' segments the scene into the dark and bright image objects based on a threshold value that maximizes the contrast between them [113]. The algorithm utilizes the optimal threshold separately for each image object which initiates a chessboard segmentation of variable scale and then performs the split on each square [114,115]. It was found quite helpful to identify the shadows, pathways, and pavements between the tree crowns.

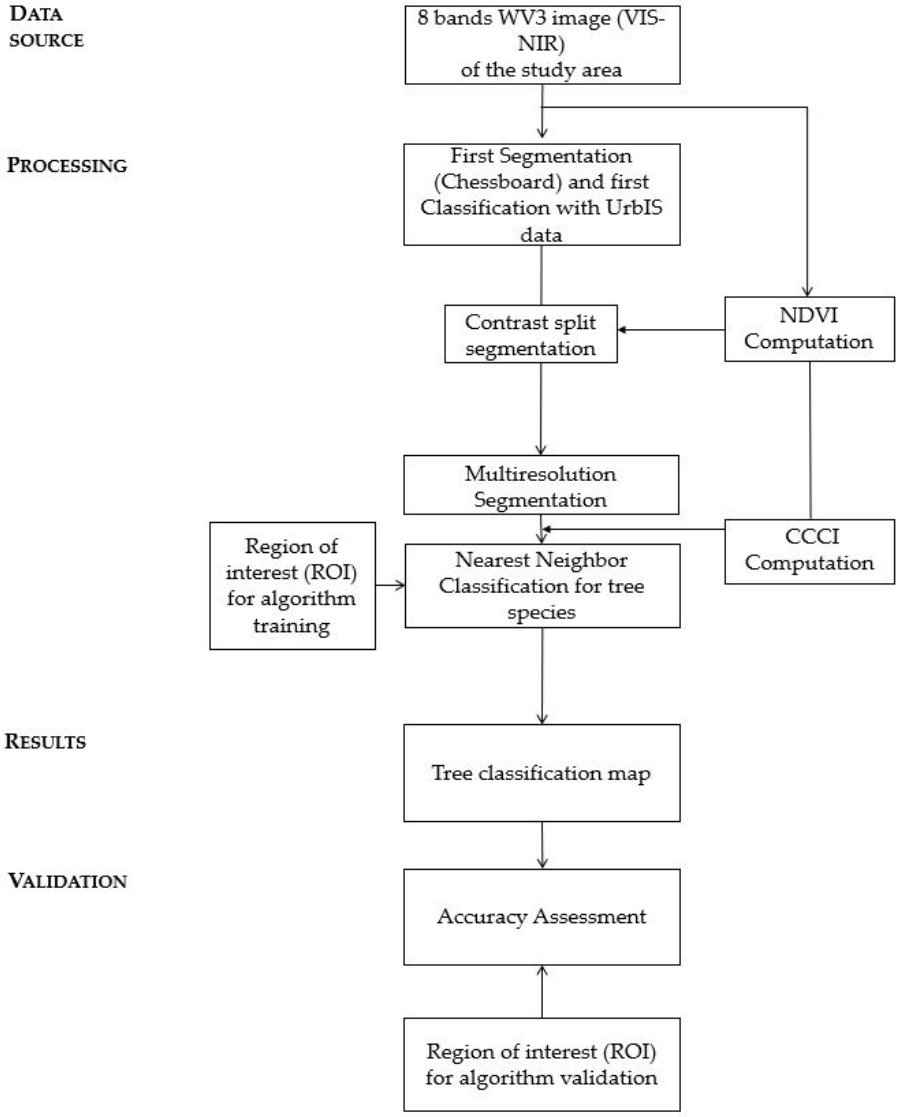

Figure 3. The Geospatial Object-Based Image Analysis (GEOBIA) approach of tree classification utilizing Trimble eCognition Developer® 9 platform in Brussels.

Subsequently, the multiresolution segmentation (MRS) algorithm [116] was performed to group contiguous pixels into areas (i.e., segments) geometrically and radiometrically homogenous. The MRS algorithm was set by tuning the following parameters such as the "smoothness/compactness" that determines the preferred shape of segments, and the "colour/shape" parameter that controls the weights of spectral and shape information in the calculation of segments heterogeneity [48,94,117,118]. Considering the study of Choudhury et al. [36], green areas and streets have been identified with very large objects (as the size of the shapefile polygons) and have been classified separately from the rest. In these areas, a subsequent multiresolution segmentation had been applied to have the smaller objects. For this segmentation, rather than the thematic layers, the spectral information and the geometric information of WV-3 bands have been considered. The segmentation was done several times utilizing a different number of values for each parameter. For scale, the values were within 5 to 30, whereas for the shape and compactness, the values were between 0.1 to 0.9 [48,94,117,118]. After several attempts with different values, the ideal values utilized for segmentation, were found as scale parameter = 10, shape = 0.5 and the compactness = 0.8.

Before starting the Nearest Neighbour (NN) approach, an index known as Canopy Content Chlorophyll Index (CCCI) is used to separate the grasses from the vegetation class. This index can be calibrated as follows,

$$CCCI = NDRE/NDVI2$$

where,

Normalized Difference Red Edge index [119]

NDRE = NIR2 − Red Edge/NIR2 + Red Edge,

NDVI2 = NIR2 − Red/NIR2 + Red

Then the Nearest Neighbour (NN) algorithm [120] was performed, which is a supervised classification technique that classified all objects in the entire image based on the selected samples and the defined statistics [94]. For the sample selection and algorithm training, the sample plots had been considered. Once the algorithm training had been done, classification was initiated utilizing the "Assign class" algorithm. Three dominant tree species have been classified, such as *Tilia* spp. L., *Acer* spp. L. and *Aesculus hippocastanum* L. [121] covering the whole study area in Brussels. In this case, the larger and intensely green parks were not considered as it was hardly possible to differentiate crowns from a mixed or overlapped tree species population. Moreover, those trees could not be considered in further CS (AGB estimation) mapping due to the larger difference between the street and the park environment concerning tree health issues.

Validation of the classification outcomes (Table 2) had also been done at the Trimble eCognition Developer® 9 platform [112] using confusion matrices [122–124] which is usually applied to compare the true classes with the ones assigned by the classifier on the generated maps. During the validation, 10%–15% of the total area for each class had been chosen as "true samples", as known species or classes, to train the algorithm. The estimated producer accuracy shows the completeness of classification, and the user accuracy indicates the correctness of the classes [36,125], while the Hellden parameter is used to estimate the mean accuracy for each class. The mean accuracy for each class i can be calculated using the equation presented in [36,126]:

$$\text{Mean accuracy (i)} = \frac{2A}{B+C}100\%$$

where A is the number of correctly classified reference points for class i, B is the total number of reference points in class i in the reference data, and C is the total number of reference points classified into class i.

Table 2. Validation results expressed in percentage for the trees in Brussels.

	***Acer* spp.**	***Tilia* spp.**	***Aesculus hippocastanum***
PA [1]	0.80	0.69	0.67
UA [1]	1	0.69	0.61
Hellden	0.89	0.69	0.64
KIA per Class	0.77	0.42	0.5
Overall Accuracy	0.71		
KIA	0.53		

[1] PA: Producer Accuracy, UA: User Accuracy.

In Table 2, KIA known as Kappa Index of Agreement (or Cohen's kappa coefficient), estimates the proportion of agreements [36,127]. Moreover, the overall accuracy (OA) has been estimated, which is the ratio of the sum of diagonal values of the confusion matrix to the total number of cell counts in the matrix [36,128].

2.2.2. Carbon Stock (CS) Mapping

Several studies suggest that tree AGB is the most visible, dominant, dynamic, and essential pool of the terrestrial ecosystem [8,129–131], constituting around 30% of the total terrestrial ecosystem carbon pool [132]. In this study, based on the relationships among the WV-3 (NDVI) data and LiDAR (CHM) data derived variables and the field data, the predictive AGB estimation and, eventually, CS mapping has been done in both cases (Figure 4).

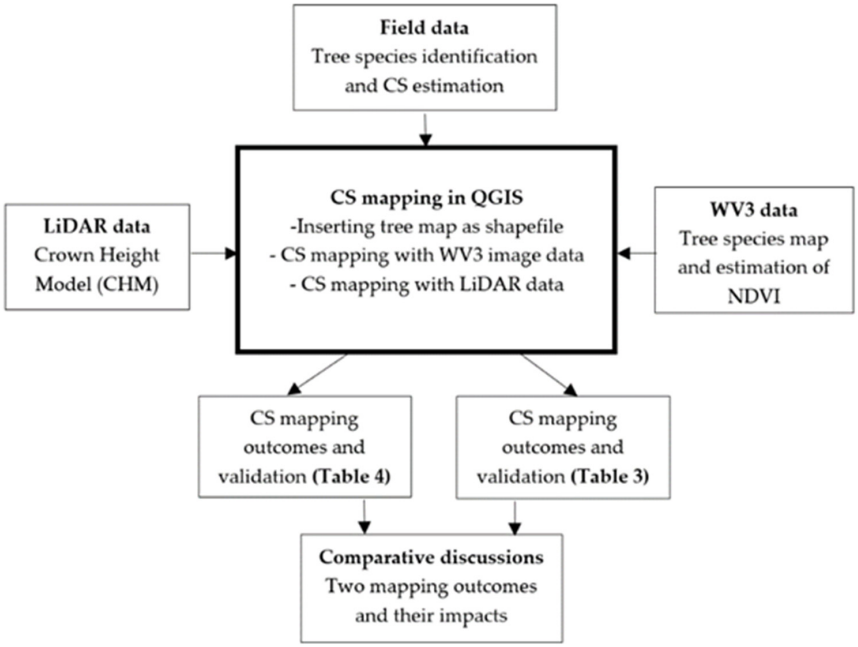

Figure 4. The overall methodology of Carbon Stock (CS) mapping, based on the combined use of CHM and NDVI, in the urban area of Brussels.

At first, the total AGB was calculated based on the field data (i.e., DBH, H, tree species, etc.) for each of the sample plots. For this calculation, an allometric model [133] was implied to calculate the AGB for each plot. The mean AGB/plot estimation was necessary as it is recommended that the tree above ground CS is assumed to be 50% of the total AGB [134–138]. Then to estimate the mean CS/plot, the mean AGB/plot was multiplied by 0.5 as a conversion factor [139–141]. Then in QGIS utilizing the WV-3 image data (from 2017, see Section 3.2.1 for details), the NDVI (Red edge and NIR1 band) of the whole study area was computed. The NDVI layer was considered in this study for the CS prediction and mapping, as previous studies claimed to find a strong correlation between the NDVI and total AGB of the trees [11,142–144]. In the case of LiDAR data, the CHM was utilized to map the CS for the dominant tree species.

Then the NDVI-derived metrics were extracted for the sample plots utilizing the "Zonal statistics" plugin [145] at the QGIS interface. The CHM-derived matrices had been computed in the case of available LiDAR data (from 2015, see Section 3.2.2 for details). After that, the linear regression models were created in a Microsoft® Excel™ spreadsheet, calibrating the correlation between the mean CS/plot and the NDVI derived metrics to find out the best model to estimate and map the CS covering the whole study area [36]. The CHM-derived matrices have also been done to determine the best model concerning the perspective CS mapping. A fishnet of 100 m^2 (10 × 10 m) resolution (as for the sample plots) was built in QGIS for both cases (NDVI and CHM) to recognize the minimum to maximum CS zones, based on the dominant species map (exported as a shapefile in QGIS) obtained from the WV-3 image data. The classification shapefile was essential to define the regions of interest, providing QGIS to map the estimated CS values considering only the

dominant tree species [36]. Otherwise, the map will show the CS values for other areas, i.e., the area covered with grass or even in an area where there is no vegetation.

Then, to validate the mapping outcomes, 20 randomly selected plots have been utilized in both cases (NDVI and CHM). This time the linear regression models were created only for the validation plots. Therefore, the differences (Tables 3 and 4) among the QGIS computed CS values, and the ground truth-values were shown to recognize the methodology's effectiveness. The validation plots were the same in both cases, which was necessary to compare the impacts and to discuss the prospects and convenience of CS mapping in urban areas (see Section 4.2 for details).

Table 3. The results obtained during the validation of estimated CS in the validation plots.

Plot ID	Tree Species	Mean CS (Field Estimation) kg/Plot	CS in QGIS Estimation (kg/Plot)	Difference (Field and QGIS)
1	*Acer* spp.	689.49	426.0	263.49
2	*Acer* spp.	930.91	397.8	533.11
3	*Acer* spp.	224.04	285.0	60.96
4	*Aesculus hippocastanum*	216.95	581.1	364.15
5	*Tilia* spp.	302.25	158.2	144.05
6	*Acer* spp.	534.17	355.5	178.67
7	*Tilia* spp.	277.49	411.9	134.41
8	*Acer* spp.	188.18	31.3	156.88
9	*Acer* spp.	332.73	242.8	89.93
10	*Tilia* spp.	626.63	341.4	285.23
11	*Tilia* spp.	277.97	538.8	260.83
12	*Tilia* spp.	64.13	214.6	150.47
13	*Acer* spp.	698.78	397.8	300.98
14	*Aesculus hippocastanum*	641.46	341.4	300.06
15	*Tilia* spp.	112.44	271.0	158.56
16	*Acer* spp.	466.16	341.4	124.76
17	*Tilia* spp.	97.31	45.4	51.91
18	*Acer* spp.	121.50	369.6	248.10
19	*Aesculus hippocastanum*	577.99	609.3	31.31
20	*Acer* spp.	316.80	200.5	116.30

Table 4. The results obtained during the estimation of CS in the validation plots.

Plot ID	Tree Species	Mean CS (Field Estimation) kg/Plot	CS in QGIS Estimation (kg/Plot)	Difference (Field and QGIS)
1	*Acer* spp.	689.49	761.3	71.81
2	*Acer* spp.	930.91	548.6	382.31
3	*Acer* spp.	224.04	343.5	119.46
4	*Aesculus hippocastanum*	216.95	188.5	28.45
5	*Tilia* spp.	302.25	356	53.75
6	*Acer* spp.	534.17	675	140.83
7	*Tilia* spp.	277.49	283.3	5.81
8	*Acer* spp.	188.18	230.9	42.72
9	*Acer* spp.	332.73	670.3	337.57
10	*Tilia* spp.	626.63	790.2	163.57
11	*Tilia* spp.	277.97	462.6	184.63
12	*Tilia* spp.	64.13	57.6	6.53
13	*Acer* spp.	698.78	696.9	1.88
14	*Aesculus hippocastanum*	641.46	179	462.46
15	*Tilia* spp.	112.44	200.2	87.76
16	*Acer* spp.	466.16	464.5	1.66
17	*Tilia* spp.	97.31	188.3	90.99
18	*Acer* spp.	121.5	93.9	27.6
19	*Aesculus hippocastanum*	577.99	599.4	21.41
20	*Acer* spp.	316.8	283.8	33

3. Results

3.1. GEOBIA Classification Results and Validation

As the WV-3 image was from the early spring, trees having dead leaves/branches made it relatively harder to identify the species in Brussels. Thus, species detection was difficult due to the spectral similarities and understory issues. However, the classified map shows that most of the streets are covered with the *Acer* spp. and *Tilia* spp., while the other species, *Aesculus hippocastanum* has been primarily observed in the southern part of the city (Figure 5).

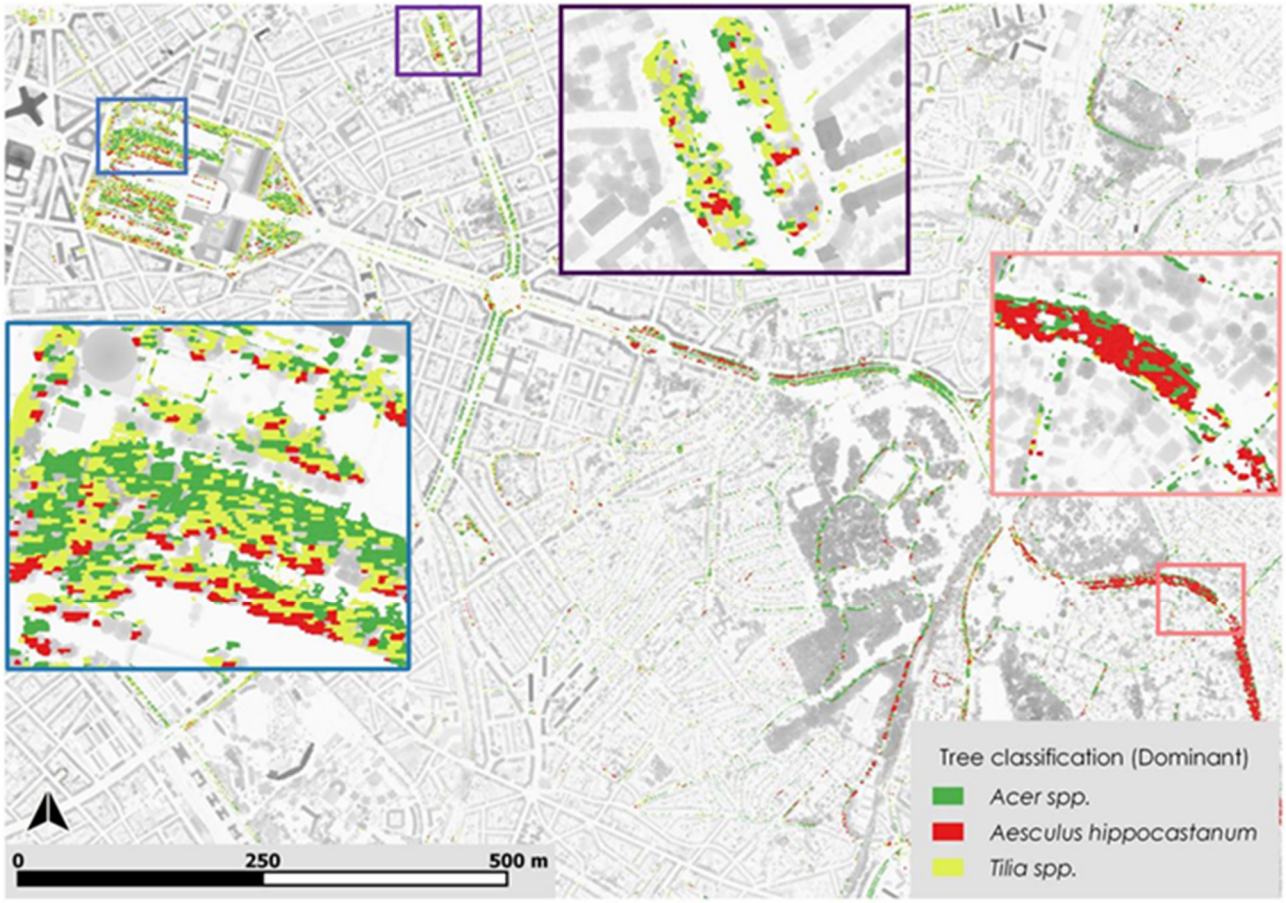

Figure 5. The figure shows the tree species classification (*Acer* spp., *Aesculus hippocastanum*, and *Tilia* spp.) obtained with the Geospatial Object-Based Image Analysis (GEOBIA) approach utilizing the WorldView-3 (WV-3) image data in the urban area of Brussels.

The producer and user accuracy were around 70% for *Tilia* spp. and *Aesculus hippocastanum*, and around 80% to 100% were for the *Acer* spp. during the confusion matrix estimation (Table 2). Indeed, it was quite essential to define the effectiveness of the GEOBIA approach and to show the percentage of error.

3.2. CS Mapping and Validation

3.2.1. CS Mapping in Brussels with WV-3 Image Data

The computed CS for the dominant species has been mapped showing the quantity of CS based on the species in different zones (Figure 6). As far as most of the trees were on the streets, the canopies were not overlapped by the wider crowns. Except for some plots having trees almost leafless or trimmed canopies, the computed CS values based on NDVI derived variables were significant (Figure 6) for most of the dominant species.

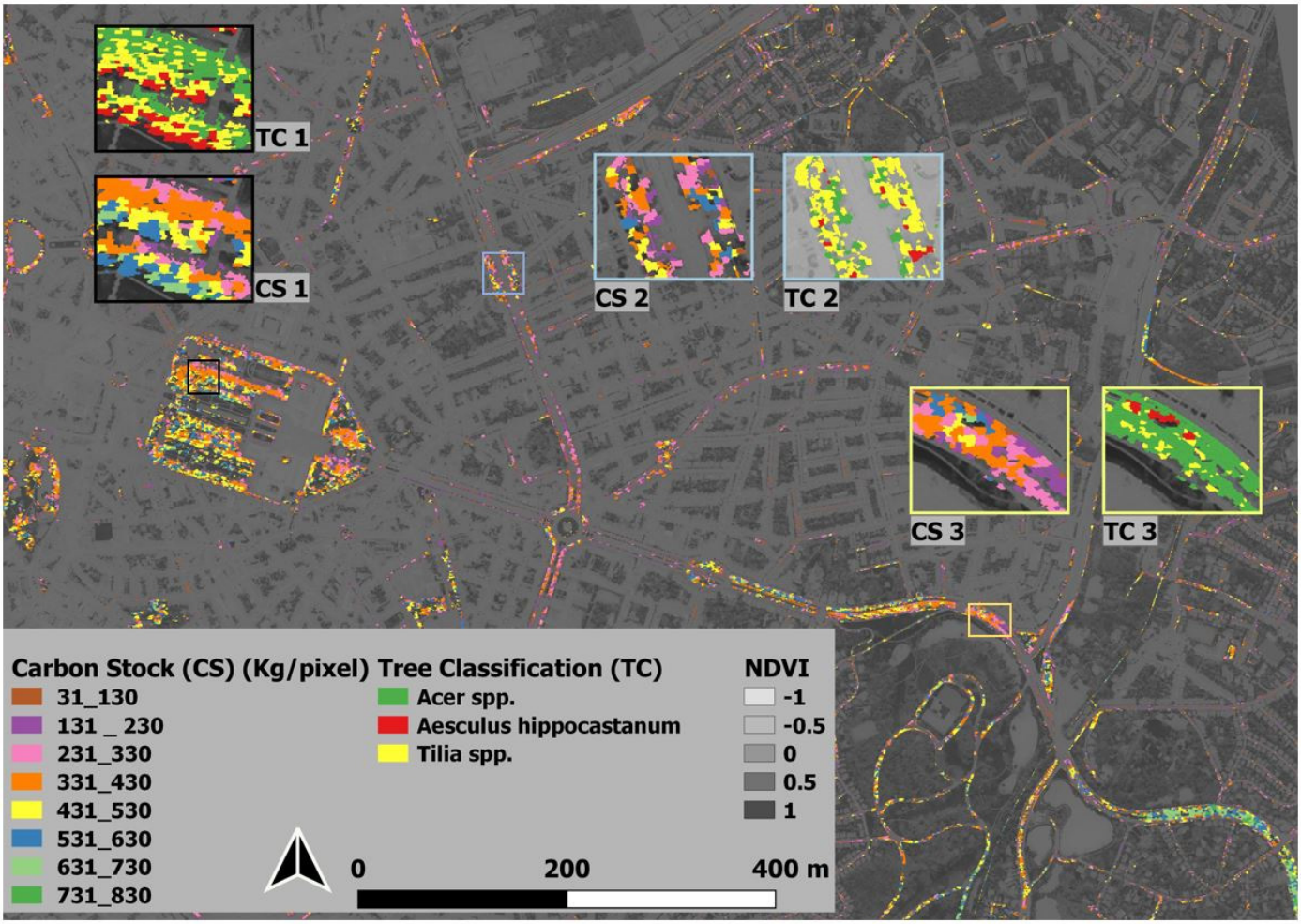

Figure 6. Mapping outcomes of the computed Carbon Stocks (CS) for the dominant tree species (*Acer* spp., *Aesculus hippocastanum*, and *Tilia* spp.) superimposed over the NDVI map in the urban area of Brussels utilizing the WorldView-3 (WV-3) image data (QGIS-NDVI).

In Figure 6, all three-square boxes (as in CS1, CS2, and CS3) are showing moderate (i.e., pink, orange, yellow, and blue coloured zones) to a higher quantity of CS for each of the species (as in TC1, TC2, and TC3). These three zones were zoomed-in considering those plots having comparatively dense canopies, as the WV-3 image was acquired in early spring, most of the plots were with lighter crowns or leaves.

In Table 3, the validation results show that the field estimation and QGIS computed CS values have apparent variations in few cases. These kinds of differences between the field estimated and the computed values were quite natural in the case of this study. The field data were collected in the summer of 2019, while the WV-3 image was acquired in the early spring of 2017. QGIS computation was done based on the NDVI (WV-3 data) extracted values where most of the trees were leafless or less green. As a result, in the case of few plots, NDVI values were lower, which indeed showed lower CS values during the mapping. In addition, the year gap between the field data (2019) and the WV-3 data (2017) also significantly impacted the CS mapping outcomes, since trees in urban areas usually go through the management practices (i.e., trimming, pruning, etc.) [146], which is also responsible for the larger variations among the field and QGIS computed values (Table 3). For instance, out of the 20 validation plots, only three plots (plot no. 4, 11, and 18) are showing noticeably more CS/plot than those of the field estimations. Trees in those plots are assumed to be a subject of trimming and or other management practices, explaining the reasons for having lower AGB or CS/plot in 2019 than those of 2017 for those three plots. A

regression analysis had been done to understand the significance of the mapping approach. It was quite noticeable that in most cases where the tree canopies were comparatively evident, even in the early spring season, the percentage of agreement (Figure 7) was more than 80% (R^2 = 0.83). Except for a few cases, this CS mapping approach could be applied in CS mapping, even in a complex urban environment.

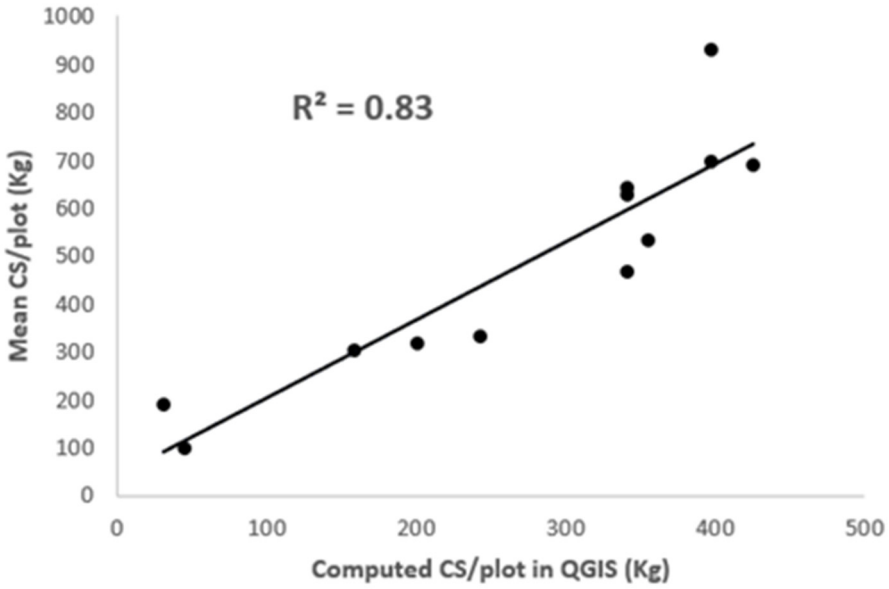

Figure 7. Linear correlation between field estimations and QGIS computations during the validation of the Carbon Stocks (CS) mapping in Brussels.

3.2.2. CS Mapping in Brussels with LiDAR Data

Figure 8 shows that the computed CS map in QGIS was quite relevant in LiDAR data for all the identified dominant species (TC1, TC2, and TC3 in Figure 8). Even the LiDAR data was from 2015, each of the three dominant species had shown evident outcomes in CS mapping (CS1, CS2, and CS3 in Figure 8) based on the field data of 2019. As the LiDAR data (from summer 2015) and field data were acquired in summer, the AGB productions per plots were significant to predict the CS during the mapping based on the CHM- derived variables in QGIS.

For the CS mapping validation, the validation plots were the same ones as earlier in the case of WV-3 image data. The outcomes of the validation plots did not show that much difference between the field estimated and QGIS computed values (Table 4). Only a few plots were showing higher differences in the quantity of computed CS, which was assumed to be a result of tree crown management practices (i.e., trimming, pruning, etc.) [146]. Out of all 20 plots, only a few plots (i.e., plot no. 2, 9, 14, 15, and 17) were showing noticeable variations between the field and QGIS estimations (Table 4). While in most of the plots, trees were showing lower differences in the case of the total atmospheric CS considering the on-plot calibrated values.

A regression analysis was done to understand the relevance of the applied CS mapping approach. It was noticed that the R2 was significantly higher (84%), for most of the plots (Figure 9). As shown earlier (Section 3.2.1), the data acquisition period (2015 and 2019) and the certain tree crown management practices (i.e., Trimming, pruning, etc.) [146] have also been found responsible for having larger variations in a few cases. As a result of regular crown trimming practices, the trees, even with a wider trunk, were showing smaller crowns in CHM during the CS computation in QGIS.

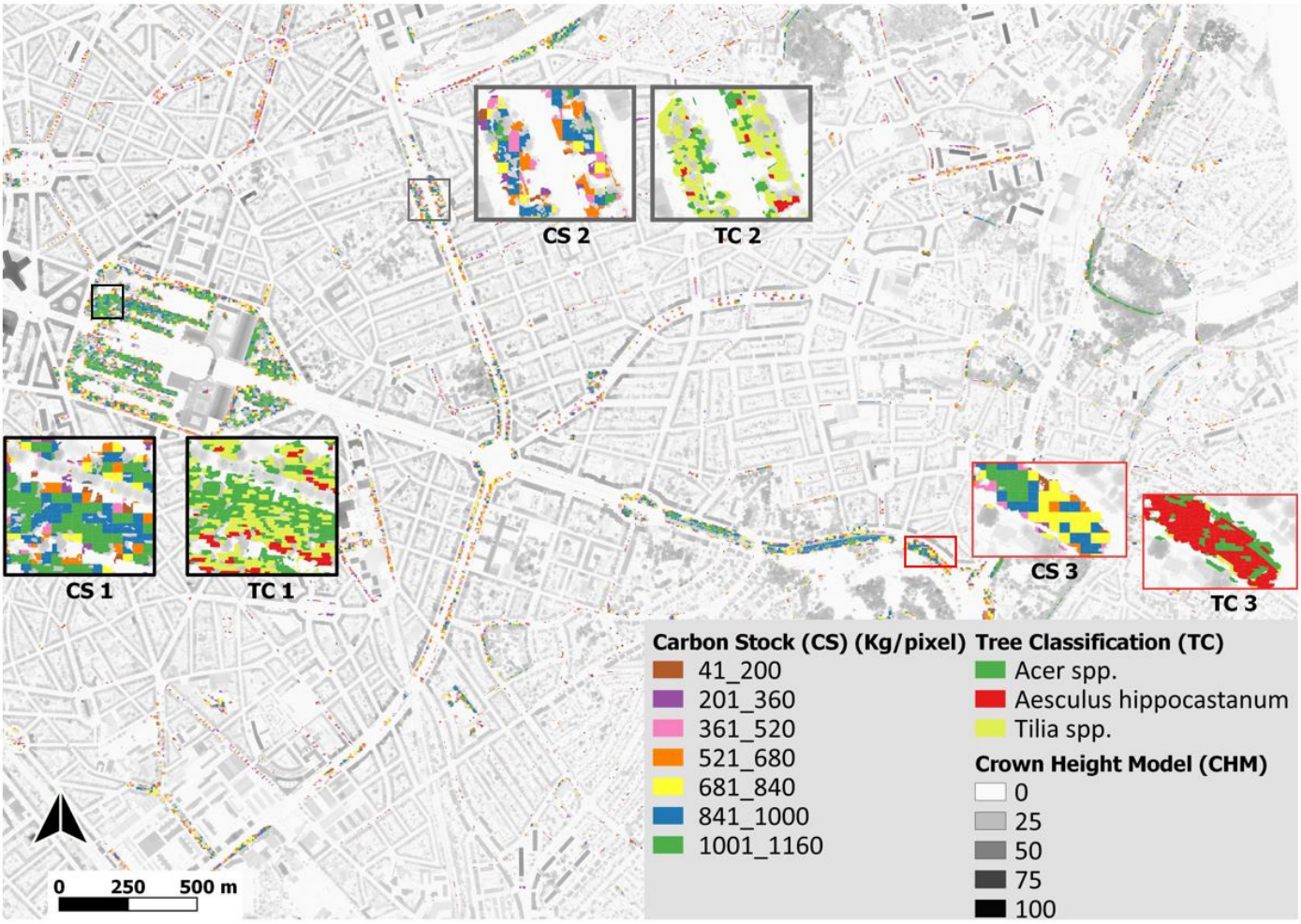

Figure 8. Mapping outcomes of the computed Carbon Stocks (CS) for the dominant tree species (*Acer* spp., *Aesculus hippocastanum*, and *Tilia* spp.) superimposed over the CHM LiDAR map in the urban area of Brussels (QGIS- CHM).

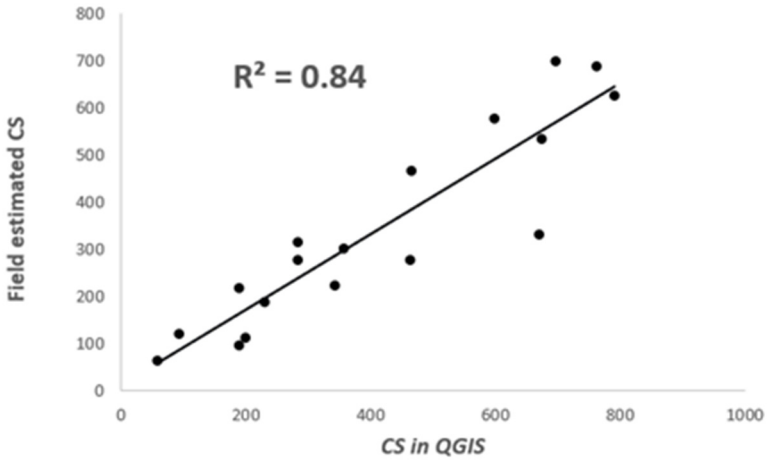

Figure 9. Linear correlation between field estimation and QGIS computation of CS/plot during the validation.

4. Discussion

4.1. GEOBIA Classification and Urban Trees

WV-3 image data were utilized to classify three dominant tree species applying the GEOBIA approach in the case of a heterogeneous urban area like as Brussels. The Overall Accuracy (OA) of the species classification was around 71%, considering all the identified urban tree species (Table 2). The classification accuracy could be improved (around 90%) by applying the data fusion (i.e., LiDAR and hyperspectral) approach or estimating OA considering the general urban land cover classification [147–153]. Since this study's primary goal was to identify and classify only the dominant tree species for further CS mapping in QGIS, we show the OA only referring to the trees class and not for the other land cover classes such as roads, grasslands, and pavements. Unfortunately, studies on urban tree species or genera-based classification (only with multispectral data) with better accuracy (more than 70%) are hardly available unless the study area is quite smaller (i.e., [154–156]). Recently, Fang et al. [157] have done the tree genera-based classification (from WV-3 data) with an OA of 62 to 74% for a larger urban area in Washington D.C., USA. Considering a study area covering almost 49 km^2, this study in Brussels also could be a good example for approving the efficacy of the GEOBIA approach. The accuracy level was different for each species, where the higher was for the Acer spp. (89%) and the lower one was found for the *Aesculus hippocastanum* (64%). Initially, the segmentation and later the relevant samples for training the NN algorithm significantly influenced the OA of the classification outcomes, as shown in previous studies [36,158]. Training samples must be sufficient considering each species/class, which will be enough for the algorithm to verify different classes. In this study, the samples had been selected to train the NN algorithm covering the whole study area in Brussels. However, the different species' spectral characteristics made it quite challenging to distinguish due to their unique phenological ages or conditions [147,159]. In some cases, misinterpretations of desired classes had been identified, recognizing the "mixed pixel issues" where some pixels were not solely covered by one homogeneous class [147,160]. Consequently, with an OA of 71%, this study does show that the WV-3 data could be more convenient, especially in urban areas, as the WV-3 image has an increased level of radiometric, geometric, and spatial (8 bands) resolution leading to classify urban trees at the species level [147,161].

Even remote sensing-based technologies are far better acceptable, the potential barriers to adopting remote sensing techniques include but are not limited to the level of specialist knowledge, the data collection time, instruments type and parameters for the acquisitions, etc. For instance, the classification OA could minimize such issues as the image registration error, the spectral and spatial resolution limitations, and overlapping spectral signature of the classes. These facts could be considered to initiate further research to improve and utilize the GEOBIA approach to achieve a species-level classification with higher accuracy, especially for the urban trees.

4.2. CS Mapping Approach: A Comparative Analysis

In this study, the mapping approach has been found far more convincing than that of the existing traditional approaches (i.e., approaches excluding remote sensing tools). The traditional biomass assessment methods are mostly based on field measurements which are not so convenient or practical to conduct over large areas considering a broad-scale assessment [8,162]. Considering the dominant species, the CS mapping outcomes in Brussels were quite explicit and feasible, where the assessment was highly influenced by the seasonal variations between the data sources (field and remote sensing data). However, no such factors or issues could hardly be sorted out to improve the mapping outcomes in both cases. For instance, it is evident that in Brussels, the CS mapping outcomes could be more significant having both data sources (i.e., field and remote sensing data) from the same season or year. The CS computation utilizing the LiDAR data could be a good example since there was not much variation with the field estimations (Table 4). However, in all cases, there were other noticeable issues such as the narrow or too wide and/or

small overlapped crowns, trimmed crowns, and so on other management practices. These issues are obvious to be considered precisely for any urban landscapes [7,63,64] that are heterogeneous in space, structurally, and functionally [44,163–165]. However, the proposed remote sensing-based methodology could be availed as more essential and applicable in the case of monitoring and mapping vegetation ecosystems and their services than that of the traditional ones.

To date, it is critical to developing a high-resolution map of tree biomass within the context of carbon monitoring over terrestrial ecosystems to assess the ecosystem response to climate change [166–171], which increases the utilization of RS-based technologies for the last few decades. For instance, LiDAR data are widely being used to complete high-resolution surveys of vegetation structure over forested areas and cities [53,172–175] and estimate biomass and carbon storage in urban vegetation [26,53,176,177] due to its improved accuracy. Even though it is believed that the application of RS is quite expensive in vegetation mapping, Jones et al. (2010) [33,178] found automated methods from combined hyperspectral and LiDAR data (approximately USD 6 per ha) to be competitive against traditional aerial photograph interpretation (approximately USD 12 per ha) in terms of accuracy and cost for a study area in South-western Canada. However, the availability of LiDAR data is not always cost-effective, especially for developing countries. For those cases where LiDAR data are hardly available, high-resolution image data could be a solution for the city policymakers. For instance, studies show that high-resolution commercial data (Rapid Eye, IKONOS, Geo-eye) are available with an approximate cost of 1–14 € per km^2, which is still more affordable than the LiDAR data (USD 62–240 per km^2) [179,180]. According to Hummel et al., the approximate cost of aerial LiDAR data acquisition for an area of almost 128 km^2 (31,614 acres) was around USD 40,500, excluding the processing costs (additional USD 33,424) [181]. While the WV-3 image data covering an area of 128 km^2 could be around USD 2500 (USD 19 km^{-2}), considering the best possible buying options for archive imagery [182]. This could be an appropriate example of LiDAR data's application of almost 15 to 20 times higher than that of the WV-3 image data. Therefore, it could be a better initiative to imply other data sources, especially in developing countries, where it is impossible to integrate or have an available LiDAR data source. Considering the cost-efficiency and the research perspectives, this study has been conducted to identify the best outcomes in each case (LiDAR and WV-3 image data) and understand the result discrepancies among similar study areas. However, it is also clear that the mapping outcomes utilizing LiDAR data were more impressive (Table 4) than that of the WV3 data. Nevertheless, the regression analysis still showed a significant level of acceptance (Figure 7) for the WV-3 image outcomes in Brussels. On the other hand, the percentage of LiDAR data outcomes except for only a few plots was more than 80% (Figure 9).

Moreover, city planners and managers usually plan to rely on a few urban tree attributes i.e., urban forest structure, green cover, species composition and diversity, available planting spaces, and tree condition to make short- and long-term decisions about the urban forest resource [15]. However, at the same time, the costs associated with data collection and monitoring (such as remote sensing applications) have to be compensated by reducing field measurement expenses or increasing management efficiency that leads to increased income based on improved decision-making [33]. Therefore the utilization and application of the advanced remote sensing technology depend on the purpose, economic feasibility, and the prospects of the resulted outcomes. Nevertheless, the proper understanding of the urban tree species contributions in atmospheric carbon sequestration and storage is one the most pertinent issues for urban green planning and management [183,184].

5. Conclusions

This mapping approach could be an efficient tool in CS mapping that will assist urban planners in ensuring proper utilization of the available green spaces considering other valuable prospects of tree species mapping in a complex city environment. This study will also recognize the prospects of the applied approach based on an efficient

GEOBIA classification method for urban tree species mapping. For instance, this study shows that the OA of tree species classification could be hugely influenced by the trees' positions, crown structures, and spectral attributes, where the resulting outcomes were useful for further CS mapping in Brussels. The CS mapping approach reveals that the tree stands level and temporal variations of the data acquisition period might significantly impact the total atmospheric CS for each species in urban areas. This study highlights that accurate tree CS mapping is crucial for estimating and identifying the dominant species contributing a significant level of atmospheric CS, which could be an efficient support for the urban planners and environmental policymakers in planning further urban air quality assessments. It also illustrates the facts considering the convenience and suitability of utilizing LiDAR and WV3 image data, especially in the case of vegetation mapping along with their functional attributes. This study could assist future research in either case of tree classification or mapping ecosystem services, having a significant prospect on remote sensing applications in the case of heterogeneous urban areas. Especially for the developing countries or where the application of LiDAR data is not that cost-effective, this mapping approach will show the alters with WV-3 image data. Soon another study will be introduced to compare the CS mapping outcomes between the WV-3 data and the Sentinel 3 data in the case of urban trees.

This study will contribute to a better understanding of the methodology in mapping structural and functional properties, such as tree CS, as well as predicting the possible urban CS in typical city areas. It might be a way out for the policymakers in mapping tree species as well as their probable ecological significance in urban areas over the traditional methods. Thus, the researchers and city planners could go forward to employ and implement the advanced ways of CS mapping for the typical urban areas assessing the possible prospects of the approach against the unavoidable impacts of climate change.

Author Contributions: Conceptualization, M.A.M.C., A.G. and E.M.; methodology, M.A.M.C..; software, M.A.M.C. and G.M.; validation, M.A.M.C.; formal analysis, M.A.M.C., A.G., G.M. and E.M.; investigation, M.A.M.C., A.G., G.M. and E.M.; resources, M.A.M.C., A.G., E.M., B.S. and G.M.; data curation, M.A.M.C. and G.M.; writing—original draft preparation, M.A.M.C., A.G. and E.M.; writing—review and editing, M.A.M.C., A.G., E.M., B.S. and G.M.; supervision, A.G. and E.M. All authors have read and agreed to the published version of the manuscript.

Funding: This research received no external funding.

Conflicts of Interest: The authors declare no conflict of interest.

References

1. 2014 Revision of the World Urbanization Prospects | Latest Major Publications—United Nations Department of Economic and Social Affairs. Available online: https://www.un.org/en/development/desa/publications/2014-revision-world-urbanization-prospects.html (accessed on 5 May 2021).
2. Tzoulas, K.; Korpela, K.; Venn, S.; Yli-Pelkonen, V.; Kaźmierczak, A.; Niemela, J.; James, P. Promoting ecosystem and human health in urban areas using Green Infrastructure: A literature review. *Landsc. Urban Plan.* **2007**, *81*, 167–178. [CrossRef]
3. de Vries, S.; van Dillen, S.M.; Groenewegen, P.P.; Spreeuwenberg, P. Streetscape greenery and health: Stress, social cohesion and physical activity as mediators. *Soc. Sci. Med.* **2013**, *94*, 26–33. [CrossRef] [PubMed]
4. Doick, K.J.; Davies, H.J.; Moss, J.; Coventry, R.; Handley, P.; Vazmonteiro, M.; Rogers, K.; Simpkin, P. *The Canopy Cover of England's Towns and Cities: Baselining and Setting Targets to Improve Human Health and Well-Being*; University of Birmingham: Birmingham, UK, 2017; pp. 5–6.
5. Endreny, T.; Santagata, R.; Perna, A.; De Stefano, C.; Rallo, R.; Ulgiati, S. Implementing and managing urban forests: A much needed conservation strategy to increase ecosystem services and urban wellbeing. *Ecol. Model.* **2017**, *360*, 328–335. [CrossRef]
6. Nowak, D.J. *Assessing Urban Forest Effects and Values: New York City's Urban forest (Vol. 9)*; US Department of Agriculture, Forest Service, Northern Research Station: Madison, WI, USA, 2007.
7. Baines, O.; Wilkes, P.; Disney, M. Quantifying urban forest structure with open-access remote sensing data sets. *Urban For. Urban Green.* **2020**, *50*, 126653. [CrossRef]
8. Issa, S.; Dahy, B.; Ksiksi, T.; Saleous, N. A Review of Terrestrial Carbon Assessment Methods Using Geo-Spatial Technologies with Emphasis on Arid Lands. *Remote Sens.* **2020**, *12*, 2008. [CrossRef]
9. Jo, H.-K.; Kim, J.-Y.; Park, H.-M. Carbon reduction and planning strategies for urban parks in Seoul. *Urban For. Urban Green.* **2019**, *41*, 48–54. [CrossRef]

10. Behera, S.K.; Sahu, N.; Mishra, A.K.; Bargali, S.S.; Behera, M.D.; Tuli, R. Aboveground biomass and carbon stock assessment in Indian tropical deciduous forest and relationship with stand structural attributes. *Ecol. Eng.* **2017**, *99*, 513–524. [CrossRef]
11. Kanniah, K.D.; Muhamad, N.; Kang, C.S. Remote sensing assessment of carbon storage by urban forest. *IOP Conf. Ser. Earth Environ. Sci.* **2014**, *18*, 12151. [CrossRef]
12. Rosenfeld, A.H.; Akbari, H.; Romm, J.J.; Pomerantz, M. Cool communities: Strategies for heat island mitigation and smog reduction. *Energy Build.* **1998**, *28*, 51–62. [CrossRef]
13. Ferrini, F.; Fini, A. Sustainable Management Techniques for Trees in the Urban Areas. (2011): 1–19.
14. Steenberg, J.W.; Duinker, P.N.; Nitoslawski, S.A. Ecosystem-based management revisited: Updating the concepts for urban forests. *Landsc. Urban Plan.* **2019**, *186*, 24–35. [CrossRef]
15. Nitoslawski, S.A.; Galle, N.J.; Bosch, C.K.V.D.; Steenberg, J.W. Smarter ecosystems for smarter cities? A review of trends, technologies, and turning points for smart urban forestry. *Sustain. Cities Soc.* **2019**, *51*, 101770. [CrossRef]
16. Brack, C.L.; James, R.N.; Banks, J.C. Data Collection and Management for Tree Assets in Urban Environments. Proceeding Urban Data Management Symposium, 1999.
17. Brack, C. Pollution mitigation and carbon sequestration by an urban forest. *Environ. Pollut.* **2002**, *116*, S195–S200. [CrossRef]
18. Banks, J.; Brack, C.; James, R. Modelling changes in dimensions, health status, and arboricultural implications for urban trees. *Urban Ecosyst.* **1999**, *3*, 35–43. [CrossRef]
19. Nowak, D.J.; Crane, D.E. Carbon storage and sequestration by urban trees in the USA. *Environ. Pollut.* **2002**, *116*, 381–389. [CrossRef]
20. Nowak, D.J. Chicago's Urban Forest Ecosystem: Results of the Chicago Urban Forest—E. Gregory McPherson—Google Books. Available online: https://books.google.it/books?hl=en&lr=&id=RnT26_xGC-4C&oi=fnd&pg=PA83&ots=G9uEFurr1T&sig=4B7P3Onwpe9Qp84zgMYDsorMViw&redir_esc=y#v=onepage&q&f=false (accessed on 9 January 2021).
21. Mokany, K.; Raison, R.J.; Prokushkin, A. Critical analysis of root: Shoot ratios in terrestrial biomes. *Glob. Chang. Biol.* **2005**, *12*, 84–96. [CrossRef]
22. Achard, F.; Eva, H.D.; Stibig, H.-J.; Mayaux, P.; Gallego, J.; Richards, T.; Malingreau, J.-P. Determination of Deforestation Rates of the World's Humid Tropical Forests. *Science* **2002**, *297*, 999–1002. [CrossRef] [PubMed]
23. Brown, S. *Estimating Biomass and Biomass Change of Tropical Forests: A Primer*; Food & Agriculture Org.: Roma, Italy, 1997; Volume 134.
24. Liu, L.; Coops, N.C.; Aven, N.W.; Pang, Y. Mapping urban tree species using integrated airborne hyperspectral and LiDAR remote sensing data. *Remote Sens. Environ.* **2017**, *200*, 170–182. [CrossRef]
25. Dalponte, M.; Bruzzone, L.; Gianelle, D. Fusion of hyperspectral and LIDAR remote sensing data for classification of complex forest areas. *IEEE Trans. Geosci. Remote Sens.* **2008**, *46*, 1416–1427. [CrossRef]
26. Alonzo, M.; McFadden, J.P.; Nowak, D.J.; Roberts, D.A. Mapping urban forest structure and function using hyperspectral imagery and lidar data. *Urban For. Urban Green.* **2016**, *17*, 135–147. [CrossRef]
27. Zhang, Y.; Shen, W.; Li, M.; Lv, Y. Assessing spatio-temporal changes in forest cover and fragmentation under urban expansion in Nanjing, eastern China, from long-term Landsat observations (1987–2017). *Appl. Geogr.* **2020**, *117*, 102190. [CrossRef]
28. Zhang, M.; Du, H.; Mao, F.; Zhou, G.; Li, X.; Dong, L.; Zheng, J.; Zhu, D.; Liu, H.; Huang, Z.; et al. Spatiotemporal Evolution of Urban Expansion Using Landsat Time Series Data and Assessment of Its Influences on Forests. *ISPRS Int. J. Geo. Inf.* **2020**, *9*, 64. [CrossRef]
29. Shen, G.; Wang, Z.; Liu, C.; Han, Y. Mapping aboveground biomass and carbon in Shanghai's urban forest using Landsat ETM+ and inventory data. *Urban For. Urban Green.* **2020**, *51*, 126655. [CrossRef]
30. Ren, Z.; Zheng, H.; He, X.; Zhang, D.; Yu, X.; Shen, G. Spatial estimation of urban forest structures with Landsat TM data and field measurements. *Urban For. Urban Green.* **2015**, *14*, 336–344. [CrossRef]
31. Moser, G.; Serpico, S.B.; Benediktsson, J.A. Land-cover mapping by Markov modeling of spatial–contextual information in very-high-resolution remote sensing images. *Proc. IEEE* **2012**, *101*, 631–651. [CrossRef]
32. Praticò, S.; Solano, F.; Di Fazio, S.; Modica, G. Machine Learning Classification of Mediterranean Forest Habitats in Google Earth Engine Based on Seasonal Sentinel-2 Time-Series and Input Image Composition Optimisation. *Remote Sens.* **2021**, *13*, 586. [CrossRef]
33. Fassnacht, F.E.; Latifi, H.; Stereńczak, K.; Modzelewska, A.; Lefsky, M.; Waser, L.; Straub, C.; Ghosh, A. Review of studies on tree species classification from remotely sensed data. *Remote Sens. Environ.* **2016**, *186*, 64–87. [CrossRef]
34. Van Ewijk, K.Y.; Randin, C.F.; Treitz, P.M.; Scott, N.A. Predicting fine-scale tree species abundance patterns using biotic variables derived from LiDAR and high spatial resolution imagery. *Remote Sens. Environ.* **2014**, *150*, 120–131. [CrossRef]
35. Chambers, D.; Périé, C.; Casajus, N.; De Blois, S. Challenges in modelling the abundance of 105 tree species in eastern North America using climate, edaphic, and topographic variables. *For. Ecol. Manag.* **2013**, *291*, 20–29. [CrossRef]
36. Choudhury, A.M.; Marcheggiani, E.; Despini, F.; Costanzini, S.; Rossi, P.; Galli, A.; Teggi, S. Urban Tree Species Identification and Carbon Stock Mapping for Urban Green Planning and Management. *Forests* **2020**, *11*, 1226. [CrossRef]
37. Vauhkonen, J.; Ørka, H.O.; Holmgren, J.; Dalponte, M.; Heinzel, J.; Koch, B. *Tree Species Recognition Based on Airborne Laser Scanning and Complementary Data Sources*; Springer: Berlin/Heidelberg, Germany, 2013; Volume 27, pp. 135–156.
38. Ørka, H.O.; Dalponte, M.; Gobakken, T.; Næsset, E.; Ene, L.T. Characterizing forest species composition using multiple remote sensing data sources and inventory approaches. *Scand. J. For. Res.* **2013**, *28*, 677–688. [CrossRef]

39. Adelabu, S.; Mutanga, O.; Adam, E.E.; Cho, M.A. Exploiting machine learning algorithms for tree species classification in a semiarid woodland using RapidEye image. *J. Appl. Remote Sens.* **2013**, *7*, 073480. [CrossRef]
40. Carleer, A.; Wolff, E. Exploitation of Very High Resolution Satellite Data for Tree Species Identification. *Photogramm. Eng. Remote Sens.* **2004**, *70*, 135–140. [CrossRef]
41. Ghosh, A.; Fassnacht, F.E.; Joshi, P.K.; Koch, B. A framework for mapping tree species combining hyperspectral and LiDAR data: Role of selected classifiers and sensor across three spatial scales. *Int. J. Appl. Earth Obs. Geoinf.* **2014**, *26*, 49–63. [CrossRef]
42. Jensen, R.R.; Hardin, P.J.; Hardin, A.J. Classification of urban tree species using hyperspectral imagery. *Geocarto Int.* **2012**, *27*, 443–458. [CrossRef]
43. Somers, B.; Asner, G.P. Tree species mapping in tropical forests using multi-temporal imaging spectroscopy: Wavelength adaptive spectral mixture analysis. *Int. J. Appl. Earth Obs. Geoinf.* **2014**, *31*, 57–66. [CrossRef]
44. Qian, Y.; Zhou, W.; Pickett, S.T.A.; Yu, W.; Xiong, D.; Wang, W.; Jing, C. Integrating structure and function: Mapping the hierarchical spatial heterogeneity of urban landscapes. *Ecol. Process.* **2020**, *9*, 1–11. [CrossRef]
45. Zhou, W.; Troy, A. An object-oriented approach for analysing and characterizing urban landscape at the parcel level. *Int. J. Remote Sens.* **2008**, *29*, 3119–3135. [CrossRef]
46. Ouma, Y.O.; Tateishi, R. Urban-trees extraction from Quickbird imagery using multiscale spectex-filtering and non-parametric classification. *ISPRS J. Photogramm. Remote Sens.* **2008**, *63*, 333–351. [CrossRef]
47. Lee, D.S.; Shan, J.; Bethel, J.S. Class-Guided Building Extraction from Ikonos Imagery. *Photogramm. Eng. Remote Sens.* **2003**, *69*, 143–150. [CrossRef]
48. Johnson, B.A.; Jozdani, S.E. Identifying Generalizable Image Segmentation Parameters for Urban Land Cover Mapping through Meta-Analysis and Regression Tree Modeling. *Remote Sens.* **2018**, *10*, 73. [CrossRef]
49. Degerickx, J.; Hermy, M.; Somers, B. Mapping Functional Urban Green Types Using High Resolution Remote Sensing Data. *Sustainability* **2020**, *12*, 2144. [CrossRef]
50. Puissant, A.; Rougier, S.; Stumpf, A. Object-oriented mapping of urban trees using Random Forest classifiers. *Int. J. Appl. Earth Obs. Geoinf.* **2014**, *26*, 235–245. [CrossRef]
51. Pu, R.; Landry, S. Mapping urban tree species by integrating multi-seasonal high resolution pléiades satellite imagery with airborne LiDAR data. *Urban For. Urban Green.* **2020**, *53*, 126675. [CrossRef]
52. Pu, R.; Landry, S. A comparative analysis of high spatial resolution IKONOS and WorldView-2 imagery for mapping urban tree species. *Remote Sens. Environ.* **2012**, *124*, 516–533. [CrossRef]
53. Mitchell, M.G.; Johansen, K.; Maron, M.; McAlpine, C.; Wu, D.; Rhodes, J.R. Identification of fine scale and landscape scale drivers of urban aboveground carbon stocks using high-resolution modeling and mapping. *Sci. Total. Environ.* **2018**, *622-623*, 57–70. [CrossRef] [PubMed]
54. Caynes, R.J.C.; Mitchell, M.G.E.; Wu, D.S.; Johansen, K.; Rhodes, J.R. Using high-resolution LiDAR data to quantify the three-dimensional structure of vegetation in urban green space. *Urban Ecosyst.* **2016**, *19*, 1749–1765. [CrossRef]
55. Birdal, A.C.; Avdan, U.; Türk, T. Estimating tree heights with images from an unmanned aerial vehicle. *Geomat. Nat. Hazards Risk* **2017**, *8*, 1144–1156. [CrossRef]
56. Alonzo, M.; Bookhagen, B.; Roberts, D.A. Urban tree species mapping using hyperspectral and lidar data fusion. *Remote Sens. Environ.* **2014**, *148*, 70–83. [CrossRef]
57. Kim, S.; McGaughey, R.J.; Andersen, H.-E.; Schreuder, G. Tree species differentiation using intensity data derived from leaf-on and leaf-off airborne laser scanner data. *Remote Sens. Environ.* **2009**, *113*, 1575–1586. [CrossRef]
58. Plowright, A.A.; Coops, N.C.; Eskelson, B.N.; Sheppard, S.R.; Aven, N.W. Assessing urban tree condition using airborne light detection and ranging. *Urban For. Urban Green.* **2016**, *19*, 140–150. [CrossRef]
59. Kim, S.; Hinckley, T.; Briggs, D. Classifying individual tree genera using stepwise cluster analysis based on height and intensity metrics derived from airborne laser scanner data. *Remote Sens. Environ.* **2011**, *115*, 3329–3342. [CrossRef]
60. Ørka, H.O.; Næsset, E.; Bollandsås, O.M. Classifying species of individual trees by intensity and structure features derived from airborne laser scanner data. *Remote Sens. Environ.* **2009**, *113*, 1163–1174. [CrossRef]
61. Yao, W.; Krzystek, P.; Heurich, M. Tree species classification and estimation of stem volume and DBH based on single tree extraction by exploiting airborne full-waveform LiDAR data. *Remote Sens. Environ.* **2012**, *123*, 368–380. [CrossRef]
62. Myeong, S.; Nowak, D.J.; Hopkins, P.F.; Brock, R.H. Urban cover mapping using digital, high-spatial resolution aerial imagery. *Urban Ecosyst.* **2001**, *5*, 243–256. [CrossRef]
63. Qian, Y.; Zhou, W.; Nytch, C.J.; Han, L.; Li, Z. A new index to differentiate tree and grass based on high resolution image and object-based methods. *Urban For. Urban Green.* **2020**, *53*, 126661. [CrossRef]
64. Azeez, O.S.; Pradhan, B.; Shafri, H.Z.M.; Shukla, N.; Lee, C.H.; Rizeei, H.M. Modeling of CO emissions from traffic vehicles using artificial neural networks. *Appl. Sci.* **2019**, *9*, 313. [CrossRef]
65. Wilkes, P.; Disney, M.; Vicari, M.; Calders, K.; Burt, A. Estimating urban above ground biomass with multi-scale LiDAR. *Carbon Balance Manag.* **2018**, *13*, 10. [CrossRef]
66. Zhu, Z.; Zhou, Y.; Seto, K.C.; Stokes, E.C.; Deng, C.; Pickett, S.T.; Taubenböck, H. Understanding an urbanizing planet: Strategic directions for remote sensing. *Remote Sens. Environ.* **2019**, *228*, 164–182. [CrossRef]
67. Maynard, C.L.; Lawrence, R.L.; Nielsen, G.A.; Decker, G. Modeling Vegetation Amount Using Bandwise Regression and Ecological Site Descriptions as an Alternative to Vegetation Indices. *GISci. Remote Sens.* **2007**, *44*, 68–81. [CrossRef]

68. Kankare, V.; Vastaranta, M.; Holopainen, M.; Räty, M.; Yu, X.; Hyyppä, J.; Hyyppä, H.; Alho, P.; Viitala, R. Retrieval of Forest Aboveground Biomass and Stem Volume with Airborne Scanning LiDAR. *Remote Sens.* **2013**, *5*, 2257–2274. [CrossRef]
69. Wannasiri, W.; Nagai, M.; Honda, K.; Santitamnont, P.; Miphokasap, P. Extraction of Mangrove Biophysical Parameters Using Airborne LiDAR. *Remote Sens.* **2013**, *5*, 1787–1808. [CrossRef]
70. Lu, D. The potential and challenge of remote sensing-based biomass estimation. *Int. J. Remote Sens.* **2006**, *27*, 1297–1328. [CrossRef]
71. Foody, G.M.; Boyd, D.S.; Cutler, M. Predictive relations of tropical forest biomass from Landsat TM data and their transferability between regions. *Remote Sens. Environ.* **2003**, *85*, 463–474. [CrossRef]
72. Kobayashi, S.; Omura, Y.; Sanga-Ngoie, K.; Widyorini, R.; Kawai, S.; Supriadi, B.; Yamaguchi, Y. Characteristics of Decomposition Powers of L-Band Multi-Polarimetric SAR in Assessing Tree Growth of Industrial Plantation Forests in the Tropics. *Remote Sens.* **2012**, *4*, 3058–3077. [CrossRef]
73. Clewley, D.; Lucas, R.; Accad, A.; Armston, J.; Bowen, M.; Dwyer, J.; Pollock, S.; Bunting, P.; McAlpine, C.; Eyre, T.; et al. An Approach to Mapping Forest Growth Stages in Queensland, Australia through Integration of ALOS PALSAR and Landsat Sensor Data. *Remote Sens.* **2012**, *4*, 2236–2255. [CrossRef]
74. Robinson, C.; Saatchi, S.; Neumann, M.; Gillespie, T. Impacts of Spatial Variability on Aboveground Biomass Estimation from L-Band Radar in a Temperate Forest. *Remote Sens.* **2013**, *5*, 1001–1023. [CrossRef]
75. Zheng, D.; Rademacher, J.; Chen, J.; Crow, T.; Bresee, M.; Le Moine, J.; Ryu, S.-R. Estimating aboveground biomass using Landsat 7 ETM+ data across a managed landscape in northern Wisconsin, USA. *Remote Sens. Environ.* **2004**, *93*, 402–411. [CrossRef]
76. Coulibaly, L.; Migolet, P.; Adegbidi, H.; Fournier, R.; Hervet, E. Mapping Aboveground Forest Biomass from Ikonos Satellite Image and Multi-Source Geospatial Data using Neural Networks and a Kriging Interpolation. *Int. Geosci. Remote Sens. Symp.* **2008**, *3*, III-298. [CrossRef]
77. Castel, T. Retrieval biomass of a large Venezuelan pine plantation using JERS-1 SAR data. Analysis of forest structure impact on radar signature. *Remote Sens. Environ.* **2002**, *79*, 30–41. [CrossRef]
78. Wijaya, A.; Gloaguen, R. Fusion of ALOS Palsar and Landsat ETM data for land cover classification and biomass modeling using non-linear methods. *Int. Geosci. Remote Sens. Symp.* **2009**, *3*, III-581. [CrossRef]
79. Simple Random Sampling of Individual Items in the Absence of a Sampling Frame that Lists the Individuals | New Zealand Journal of Forestry Science | Full Text. Available online: https://nzjforestryscience.springeropen.com/articles/10.1186/s40490-016-0071-1 (accessed on 24 May 2021).
80. West, P.W. Simple random sampling of individual items in the absence of a sampling frame that lists the individuals. *N. Z. J. For. Sci.* **2016**, *46*, 1–7. [CrossRef]
81. Gregoire, T.G.; Valentine, H.T. *Sampling Strategies for Natural Resources and the Environment*; Chapman and Hall/CRC: Boca Raton, FL, USA, 2007.
82. Pinkham, R.S. An Efficient Algorithm for Drawing a Simple Random Sample. *J. R. Stat. Soc. Ser. C Appl. Stat.* **1987**, *36*, 370. [CrossRef]
83. Nikon | News | Nikon Introduces New Laser Rangefinder "Forestry 550". Available online: https://www.nikon.com/news/2008/0924_forestry_02.htm (accessed on 16 November 2020).
84. Degerickx, J.; Roberts, D.; McFadden, J.; Hermy, M.; Somers, B. Urban tree health assessment using airborne hyperspectral and LiDAR imagery. *Int. J. Appl. Earth Obs. Geoinf.* **2018**, *73*, 26–38. [CrossRef]
85. Solano, F.; Di Fazio, S.; Modica, G. A methodology based on GEOBIA and WorldView-3 imagery to derive vegetation indices at tree crown detail in olive orchards. *Int. J. Appl. Earth Obs. Geoinf.* **2019**, *83*, 101912. [CrossRef]
86. Gilbertson, J.K.; Kemp, J.; van Niekerk, A. Effect of pan-sharpening multi-temporal Landsat 8 imagery for crop type differentiation using different classification techniques. *Comput. Electron. Agric.* **2017**, *134*, 151–159. [CrossRef]
87. Karakus, P.; Karabork, H. Effect of pansharpened image on some of pixel based and object based classification accuracy. *ISPRS Int. Arch. Photogramm. Remote Sens. Spat. Inf. Sci.* **2016**, *XLI-B7*, 235–239. [CrossRef]
88. Padwick, C.; Deskevich, M.; Pacifici, F.; Smallwood, S. WorldView-2 Pan-Sharpening. In Proceedings of the ASPRS 2010 Annual Conference, San Diego, CA, USA, 26–30 April 2010; Volume 2630, pp. 1–14.
89. Geopunt.be—The Flemish Geoportal | Con Terra. Available online: https://www.con-terra.com/casestudies/geopuntbe-flemish-geoportal (accessed on 9 January 2021).
90. ERDAS IMAGINE: World-Class Remote Sensing Software | Hexagon Geospatial. Available online: https://www.hexagongeospatial.com/products/power-portfolio/erdas-imagine/erdas-imagine-remote-sensing-software-package (accessed on 9 January 2021).
91. UrbIS Download. Available online: http://urbisdownload.gis.irisnet.be/en/temporality/ (accessed on 16 November 2020).
92. Jebur, M.N.; Shafri, H.Z.M.; Pradhan, B.; Tehrany, M.S. Per-pixel and object-oriented classification methods for mapping urban land cover extraction using SPOT 5 imagery. *Geocarto Int.* **2013**, *29*, 792–806. [CrossRef]
93. Wang, L.; Sousa, W.P.; Gong, P. Integration of object-based and pixel-based classification for mapping mangroves with IKONOS imagery. *Int. J. Remote Sens.* **2004**, *25*, 5655–5668. [CrossRef]
94. Makinde, E.O.; Salami, A.; Olaleye, J.B.; Okewusi, O.C. Object Based and Pixel Based Classification Using Rapideye Satellite Imager of ETI-OSA, Lagos, Nigeria. *Geoinformatics FCE CTU* **2016**, *15*, 59–70. [CrossRef]
95. Blaschke, T.; Lang, S.; Lorup, E.; Strobl, J.; Zeil, P. Object-oriented image processing in an integrated GIS/remote sensing environment and perspectives for environmental applications. *Environ. Inf. Plan. Politics Public* **2000**, *2*, 555–570.

96. Estoque, R.C.; Murayama, Y.; Akiyama, C. Pixel-based and object-based classifications using high- and medium-spatial-resolution imageries in the urban and suburban landscapes. *Geocarto Int.* **2015**, *30*, 1113–1129. [CrossRef]
97. Li, X.; Meng, Q.; Gu, X.; Jancsó, T.; Yu, T.; Wang, K.; Mavromatis, S. A hybrid method combining pixel-based and object-oriented methods and its application in Hungary using Chinese HJ-1 satellite images. *Int. J. Remote Sens.* **2013**, *34*, 4655–4668. [CrossRef]
98. Jabari, S.; Zhang, Y. Very High Resolution Satellite Image Classification Using Fuzzy Rule-Based Systems. *Algorithms* **2013**, *6*, 762–781. [CrossRef]
99. Platt, R.V.; Rapoza, L. An Evaluation of an Object-Oriented Paradigm for Land Use/Land Cover Classification∗. *Prof. Geogr.* **2008**, *60*, 87–100. [CrossRef]
100. Wieland, M.; Pittore, M. Performance Evaluation of Machine Learning Algorithms for Urban Pattern Recognition from Multi-spectral Satellite Images. *Remote Sens.* **2014**, *6*, 2912–2939. [CrossRef]
101. Gao, Y.; Mas, J.F. 2008. A Comparison of the Performance of Pixel Based and Object Based Classifications over Images with Various Spatial Resolutions. Available online: https://medwelljournals.com/abstract/?doi=ojesci.2008.27.35 (accessed on 24 May 2021).
102. Han, R.; Liu, P.; Wang, G.; Zhang, H.; Wu, X. Advantage of Combining OBIA and Classifier Ensemble Method for Very High-Resolution Satellite Imagery Classification. *J. Sens.* **2020**, *2020*, 1–15. [CrossRef]
103. Hossain, M.D.; Chen, D. Segmentation for Object-Based Image Analysis (OBIA): A review of algorithms and challenges from remote sensing perspective. *ISPRS J. Photogramm. Remote Sens.* **2019**, *150*, 115–134. [CrossRef]
104. Kucharczyk, M.; Hay, G.; Ghaffarian, S.; Hugenholtz, C. Geographic Object-Based Image Analysis: A Primer and Future Directions. *Remote Sens.* **2020**, *12*, 2012. [CrossRef]
105. Blaschke, T. Object based image analysis for remote sensing. *ISPRS J. Photogramm. Remote Sens.* **2010**, *65*, 2–16. [CrossRef]
106. Fu, B.; Wang, Y.; Campbell, A.; Li, Y.; Zhang, B.; Yin, S.; Xing, Z.; Jin, X. Comparison of object-based and pixel-based Random Forest algorithm for wetland vegetation mapping using high spatial resolution GF-1 and SAR data. *Ecol. Indic.* **2017**, *73*, 105–117. [CrossRef]
107. Duro, D.C.; Franklin, S.; Dubé, M.G. A comparison of pixel-based and object-based image analysis with selected machine learning algorithms for the classification of agricultural landscapes using SPOT-5 HRG imagery. *Remote Sens. Environ.* **2012**, *118*, 259–272. [CrossRef]
108. Myint, S.W.; Gober, P.; Brazel, A.; Grossman-Clarke, S.; Weng, Q. Per-pixel vs. object-based classification of urban land cover extraction using high spatial resolution imagery. *Remote Sens. Environ.* **2011**, *115*, 1145–1161. [CrossRef]
109. Martins, V.S.; Kaleita, A.L.; Gelder, B.K.; da Silveira, H.L.; Abe, C.A. Exploring multiscale object-based convolutional neural network (multi-OCNN) for remote sensing image classification at high spatial resolution. *ISPRS J. Photogramm. Remote Sens.* **2020**, *168*, 56–73. [CrossRef]
110. Su, T.; Liu, T.; Zhang, S.; Qu, Z.; Li, R. Machine learning-assisted region merging for remote sensing image segmentation. *ISPRS J. Photogramm. Remote Sens.* **2020**, *168*, 89–123. [CrossRef]
111. De Pinho, C.M.D.; Fonseca, L.M.G.; Korting, T.S.; Almeida, C.; Kux, H.J.H. Land-cover classification of an intra-urban environment using high-resolution images and object-based image analysis. *Int. J. Remote Sens.* **2012**, *33*, 5973–5995. [CrossRef]
112. AGD. *ECognition Version 5 Object Oriented Image Analysis User Guide*; AGD: Munich, Germany, 2005.
113. Basic Rule Set Editing. Available online: https://docs.ecognition.com/v9.5.0/eCognition_documentation/UserGuideDeveloper/4BasicRuleSetEditing.htm (accessed on 17 November 2020).
114. El-Naggar, A.M. Determination of optimum segmentation parameter values for extracting building from remote sensing images. *Alex. Eng. J.* **2018**, *57*, 3089–3097. [CrossRef]
115. Huang, J.; Zhang, X.; Xin, Q.; Sun, Y.; Zhang, P. Automatic building extraction from high-resolution aerial images and LiDAR data using gated residual refinement network. *ISPRS J. Photogramm. Remote Sens.* **2019**, *151*, 91–105. [CrossRef]
116. Multiresolution Segmentation: An Optimization Approach . . . /Multiresolution-Segmentation-An-Optimization-Approach.pdf/ PDF4PRO. Available online: https://pdf4pro.com/view/multiresolution-segmentation-an-optimization-approach-598443.html (accessed on 19 May 2021).
117. Modica, G.; Messina, G.; De Luca, G.; Fiozzo, V.; Praticò, S. Monitoring the vegetation vigor in heterogeneous citrus and olive orchards. A multiscale object-based approach to extract trees' crowns from UAV multispectral imagery. *Comput. Electron. Agric.* **2020**, *175*, 105500. [CrossRef]
118. Benz, U.C.; Hofmann, P.; Willhauck, G.; Lingenfelder, I.; Heynen, M. Multi-resolution, object-oriented fuzzy analysis of remote sensing data for GIS-ready information. *ISPRS J. Photogramm. Remote Sens.* **2004**, *58*, 239–258. [CrossRef]
119. Carneiro, F.M.; Furlani, C.E.A.; Zerbato, C.; De Menezes, P.C.; Gírio, L.A.D.S. Correlations among vegetation indices and peanut traits during different crop development stages. *Eng. Agríc.* **2019**, *39*, 33–40. [CrossRef]
120. Blanzieri, E.; Melgani, F. Nearest Neighbor Classification of Remote Sensing Images with the Maximal Margin Principle. *IEEE Trans. Geosci. Remote Sens.* **2008**, *46*, 1804–1811. [CrossRef]
121. Blunt, W. *Linnaeus: The Compleat Naturalist*; Princeton University Press: Princeton, NJ, USA, 2001; Available online: https://www.worldcat.org/title/linnaeus-the-compleat-naturalist/oclc/1159631211?referer=di&ht=edition (accessed on 24 May 2021).
122. Gupta, D.L.; Malviya, A.K.; Singh, S. Performance Analysis of Classification Tree Learning Algorithms. *Int. J. Comput. Appl.* **2012**, *55*, 39–44. [CrossRef]
123. Immitzer, M.; Vuolo, F.; Atzberger, C. First Experience with Sentinel-2 Data for Crop and Tree Species Classifications in Central Europe. *Remote Sens.* **2016**, *8*, 166. [CrossRef]

124. So-In, C.; Mongkonchai, N.; Aimtongkham, P.; Wijitsopon, K.; Rujirakul, K. An evaluation of data mining classification models for network intrusion detection. In Proceedings of the 2014 Fourth International Conference on Digital Information and Communication Technology and its Applications (DICTAP), Bangkok, Thailand, 6–8 May 2014; pp. 90–94.
125. Foody, G.M. Assessing the Accuracy of Remotely Sensed Data: Principles and Practices. *Photogramm. Rec.* **2010**, *25*, 204–205. [CrossRef]
126. Helldén, U. *A Test of Landsat-2 Imagery and Digital Data for Thematic Mapping Illustrated by an Environmental Study in Northern Kenya*; Lund University: Lund, Sweden, 1980.
127. Cohen, J. Weighted kappa: Nominal scale agreement provision for scaled disagreement or partial credit. *Psychol. Bull.* **1968**, *70*, 213–220. [CrossRef] [PubMed]
128. Banko, G. *A Review of Assessing the Accuracy of Classifications of Remotely Sensed Data and of Methods Including Remote Sensing Data in Forest Inventory*; IIASA Interim Report; IIASA: Laxenburg, Austria, 1998; IR-98-081.
129. Gallaun, H.; Zanchi, G.; Nabuurs, G.J.; Hengeveld, G.; Schardt, M.; Verkerk, P.J. EU-wide maps of growing stock and above-ground biomass in forests based on remote sensing and field measurements. *For. Ecol. Manag.* **2010**, *260*, 252–261. [CrossRef]
130. Cairns, M.A.; Brown, S.; Helmer, E.H.; Baumgardner, G.A. Root biomass allocation in the world's upland forests. *Oecologia* **1997**, *111*, 1–11. [CrossRef] [PubMed]
131. Fonton, N.H.; Medjibé, V.; Djomo, A.; Kondaoulé, J.; Rossi, V.; Ngomanda, A.; Maïdou, H. Analyzing Accuracy of the Power Functions for Modeling Aboveground Biomass Prediction in Congo Basin Tropical Forests. *Open J. For.* **2017**, *07*, 388–402. [CrossRef]
132. Kumar, L.; Sinha, P.; Taylor, S.; AlQurashi, A.F. Review of the use of remote sensing for biomass estimation to support renewable energy generation. *J. Appl. Remote Sens.* **2015**, *9*, 097696. [CrossRef]
133. Tabacchi, G.; Cosmo, D.; Gasparini, L. Aboveground tree volume and Phytomass Prediction Equations for Forest Species in Italy. *Eur. J. For. Res.* **2011**, *130*, 911–934. [CrossRef]
134. Goslee, K.; Walker, S.M.; Grais, A.; Murray, L.; Casarim, F.; Brown, S. *Leaf Technicial Guidance Series for the Development of a Forest Carbon Monitoring System for REDD+: Module C-CS: Calculations for Estimating Carbon Stocks*; Winrock International: Morrilton, AR, USA, 2010.
135. Biomass, B.S.E. And Biomass Change of Tropical Forests: A Primer. *Rome FAO For. Pap.* **1986**, *134*.
136. Losi, C.J.; Siccama, T.G.; Condit, R. Analysis of Alternative Methods for Estimating Carbon Stock in Young Tropical Plantatiions. *For. Ecol. Manag.* **2003**, *184*, 355–368. [CrossRef]
137. Vashum, K.T.; Jayakumar, S. Methods to Estimate Above-Ground Biomass and Carbon Stock in Natural Forests-a Review. *J. Ecosyst. Ecography* **2012**, *2*, 1–7. [CrossRef]
138. Whittaker, R.H. Carbon in the Biota. In Woodwell GM, Pecan EV, Carbon in the biosphere. In Proceedings of the 24th Brookhaven Symposium in Biology, New York, NY, USA, 16–18 May 1972; pp. 281–302.
139. Food and Agriculture Organization. *Food and Agriculture Organization of the United Nations. Retrieved*; Food and Agriculture Organization: Rome, Italy, 2010; p. 2012.
140. Vicharnakorn, P.; Shrestha, R.P.; Nagai, M.; Salam, A.P.; Kiratiprayoon, S. Carbon Stock Assessment Using Remote Sensing and Forest Inventory Data in Savannakhet, Lao PDR. *Remote Sens.* **2014**, *6*, 5452–5479. [CrossRef]
141. Panel, I. *On Climate Change (IPCC)*; Cambridge University Press: Cambridge, UK, 2007.
142. Rahetlah, B.V.; Salgado, P.; Andrianarisoa, B.; Tillard, E.; Razafindrazaka, H.; Le Mezo, L.; Ramalanjaona, V.L. 2014. Relationship between Normalized Difference Vegetation Index (NDVI) and Forage Biomass Yield in the Vakinankaratra Region, Madagascar.
143. Goswami, S.; Gamon, J.; Vargas, S.; Tweedie, C. Relationships of NDVI, Biomass, and Leaf Area Index (LAI) for Six Key Plant Species in Barrow, Alaska. *PeerJ Prepr.* **2015**, *19*.
144. Coelho, A.P.; Rosalen, D.L.; De Faria, R.T. Vegetation indices in the prediction of biomass and grain yield of white oat under irrigation levels. *Pesquisa Agropecuária Tropical* **2018**, *48*, 109–117. [CrossRef]
145. Jung, M. 2013. LecoS-A QGIS plugin for automated landscape ecology analysis (No. e116v2). *PeerJ* **2013**. [CrossRef]
146. Jacobs. *Annual Report*. 2018. Available online: https://www.jacobs.com/sites/default/files/files/2018-12/Jacobs-2018-Annual-Report.pdf (accessed on 24 May 2021).
147. Jombo, S.; Adam, E.; Byrne, M.J.; Newete, S.W. Evaluating the capability of Worldview-2 imagery for mapping alien tree species in a heterogeneous urban environment. *Cogent Soc. Sci.* **2020**, *6*, 1754146. [CrossRef]
148. Lumnitz, S.; Devisscher, T.; Mayaud, J.R.; Radic, V.; Coops, N.C.; Griess, V.C. Mapping trees along urban street networks with deep learning and street-level imagery. *ISPRS J. Photogramm. Remote Sens.* **2021**, *175*, 144–157. [CrossRef]
149. Wang, M.; Liu, R.; Lu, X.; Ren, H.; Chen, M.; Yu, J. The use of mobile lidar data and Gaofen-2 image to classify roadside trees. *Meas. Sci. Technol.* **2020**, *31*, 125005. [CrossRef]
150. He, S.; Du, H.; Zhou, G.; Li, X.; Mao, F.; Zhu, D.; Xu, Y.; Zhang, M.; Huang, Z.; Liu, H.; et al. Intelligent Mapping of Urban Forests from High-Resolution Remotely Sensed Imagery Using Object-Based U-Net-DenseNet-Coupled Network. *Remote Sens.* **2020**, *12*, 3928. [CrossRef]
151. Rasti, B.; Ghamisi, P.; Gloaguen, R. Fusion of Multispectral LiDAR and Hyperspectral Imagery. In Proceedings of the IGARSS 2020—2020 IEEE International Geoscience and Remote Sensing Symposium; Institute of Electrical and Electronics Engineers (IEEE), Online, 24 February 2020; pp. 2659–2662.

152. Zhang, Y.; Shao, Z. Assessing of Urban Vegetation Biomass in Combination with LiDAR and High-resolution Remote Sensing Images. *Int. J. Remote Sens.* **2021**, *42*, 964–985. [CrossRef]
153. Hansch, R.; Hellwich, O. Fusion of Multispectral LiDAR, Hyperspectral, and RGB Data for Urban Land Cover Classification. *IEEE Geosci. Remote Sens. Lett.* **2021**, *18*, 366–370. [CrossRef]
154. Li, D.; Ke, Y.; Gong, H.; Li, X. Object-Based Urban Tree Species Classification Using Bi-Temporal WorldView-2 and WorldView-3 Images. *Remote Sens.* **2015**, *7*, 16917–16937. [CrossRef]
155. Nölke, N. Continuous Urban Tree Cover Mapping from Landsat Imagery in Bengaluru, India. *Forests* **2021**, *12*, 220. [CrossRef]
156. Mustafa, Y.; Habeeb, H.N.; Stein, A.; Sulaiman, F.Y. Identification and mapping of tree species in urban areas using worldview-2 imagery. *ISPRS Ann. Photogramm. Remote Sens. Spat. Inf. Sci.* **2015**, *II-2/W2*, 175–181. [CrossRef]
157. Fang, F.; McNeil, B.E.; Warner, T.A.; Maxwell, A.E.; Dahle, G.A.; Eutsler, E.; Li, J. Discriminating tree species at different taxonomic levels using multi-temporal WorldView-3 imagery in Washington D.C., USA. *Remote Sens. Environ.* **2020**, *246*, 111811. [CrossRef]
158. Laliberte, A.S.; Koppa, J.; Fredrickson, E.L.; Rango, A. Comparison of Nearest Neighbor and Rule-based Decision Tree Classification in an Object-oriented Environment. In Proceedings of the 2006 IEEE International Symposium on Geoscience and Remote Sensing, Denver, CO, USA, 31 July–4 August 2006; pp. 3923–3926.
159. Le Louarn, M.; Clergeau, P.; Briche, E.; Deschamps-Cottin, M. "Kill Two Birds with One Stone": Urban Tree Species Classification Using Bi-Temporal Pléiades Images to Study Nesting Preferences of an Invasive Bird. *Remote Sens.* **2017**, *9*, 916. [CrossRef]
160. Salih, A.A.; Ganawa, E.-T.; Elmahl, A.A. Spectral mixture analysis (SMA) and change vector analysis (CVA) methods for monitoring and mapping land degradation/desertification in arid and semiarid areas (Sudan), using Landsat imagery. *Egypt. J. Remote Sens. Space Sci.* **2017**, *20*, S21–S29. [CrossRef]
161. Waser, L.T.; Küchler, M.; Jütte, K.; Stampfer, T. Evaluating the Potential of WorldView-2 Data to Classify Tree Species and Different Levels of Ash Mortality. *Remote Sens.* **2014**, *6*, 4515–4545. [CrossRef]
162. Kumar, L.; Mutanga, O. Remote Sensing of Above-Ground Biomass. *Remote Sens.* **2017**, *9*, 935. [CrossRef]
163. Zhou, W.; Cadenasso, M.L.; Schwarz, K.; Pickett, S.T. Quantifying Spatial Heterogeneity in Urban Landscapes: Integrating Visual Interpretation and Object-Based Classification. *Remote Sens.* **2014**, *6*, 3369–3386. [CrossRef]
164. Cadenasso, M.L.; Pickett, S.T.; McGrath, B.; Marshall, V. *Ecological Heterogeneity in Urban Ecosystems: Reconceptualized Land Cover Models as a Bridge to Urban Design*; Springer Science and Business Media LLC: Cham, Switzerland, 2013; pp. 107–129.
165. Band, L.E. *Heterogeneity in Urban Ecosystems: Patterns and Process, Ecosystem Function in Heterogeneous Landscapes*; Springer: New York, NY, USA, 2005; pp. 257–278.
166. Houghton, R.A.; House, J.I.; Pongratz, J.; Van Der Werf, G.R.; DeFries, R.S.; Hansen, M.C.; Le Quéré, C.; Ramankutty, N. Carbon emissions from land use and land-cover change. *Biogeosciences* **2012**, *9*, 5125–5142. [CrossRef]
167. Oughton, R.A.H. Aboveground Forest Biomass and the Global Carbon Balance. *Glob. Chang. Biol.* **2005**, *11*, 945–958. [CrossRef]
168. Hurtt, G.; Zhao, M.; Sahajpal, R.; Armstrong, A.; Birdsey, R.; Campbell, E.; Dolan, K.A.; Dubayah, R.; Fisk, J.P.; Flanagan, S.; et al. Beyond MRV: High-resolution forest carbon modeling for climate mitigation planning over Maryland, USA. *Environ. Res. Lett.* **2019**, *14*, 045013. [CrossRef]
169. Hurtt, G.C.; Fisk, J.; Thomas, R.Q.; Dubayah, R.; Moorcroft, P.R.; Shugart, H.H. Linking models and data on vegetation structure. *J. Geophys. Res. Space Phys.* **2010**, *115*. [CrossRef]
170. Gu, H.; Williams, C.A.; Ghimire, B.; Zhao, F.; Huang, C. High-resolution mapping of time since disturbance and forest carbon flux from remote sensing and inventory data to assess harvest, fire, and beetle disturbance legacies in the Pacific Northwest. *Biogeosciences* **2016**, *13*, 6321–6337. [CrossRef]
171. Huang, W.; Dolan, K.A.; Swatantran, A.; Johnson, K.D.; Tang, H.; O'Neil-Dunne, J.; Dubayah, R.; Hurtt, G. High-resolution mapping of aboveground biomass for forest carbon monitoring system in the Tri-State region of Maryland, Pennsylvania and Delaware, USA. *Environ. Res. Lett.* **2019**, *14*, 095002. [CrossRef]
172. Varhola, A.; Coops, N. Estimation of watershed-level distributed forest structure metrics relevant to hydrologic modeling using LiDAR and Landsat. *J. Hydrol.* **2013**, *487*, 70–86. [CrossRef]
173. Simonson, W.D.; Allen, H.D.; Coomes, D.A. Applications of airborne lidar for the assessment of animal species diversity. *Methods Ecol. Evol.* **2014**, *5*, 719–729. [CrossRef]
174. Goodwin, N.R.; Coops, N.C.; Tooke, T.R.; Christen, A.; Voogt, J. Characterizing urban surface cover and structure with airborne lidar technology. *Can. J. Remote Sens.* **2009**, *35*, 297–309. [CrossRef]
175. Alonzo, M.; Bookhagen, B.; McFadden, J.P.; Sun, A.; Roberts, D.A. Mapping urban forest leaf area index with airborne lidar using penetration metrics and allometry. *Remote Sens. Environ.* **2015**, *162*, 141–153. [CrossRef]
176. Shrestha, R.; Wynne, R.H. Estimating Biophysical Parameters of Individual Trees in an Urban Environment Using Small Footprint Discrete-Return Imaging Lidar. *Remote Sens.* **2012**, *4*, 484–508. [CrossRef]
177. Raciti, S.M.; Hutyra, L.R.; Newell, J.D. Mapping carbon storage in urban trees with multi-source remote sensing data: Relationships between biomass, land use, and demographics in Boston neighborhoods. *Sci. Total. Environ.* **2014**, *500-501*, 72–83. [CrossRef]
178. Jones, T.G.; Coops, N.C.; Sharma, T. Assessing the utility of airborne hyperspectral and LiDAR data for species distribution mapping in the coastal Pacific Northwest, Canada. *Remote Sens. Environ.* **2010**, *114*, 2841–2852. [CrossRef]
179. Wang, K.; Wang, T.; Liu, X. A review: Individual tree species classification using integrated airborne LiDAR and optical imagery with a focus on the urban environment. *Forests* **2019**, *10*, 1. [CrossRef]

180. Ørka, H.O.; Hauglin, M. Use of Remote Sensing for Mapping of Non-Native Conifer Species. INA fagapport 33. 76p. 2016. Available online: http://www.umb.no/statisk/ina/publikasjoner/fagrapport/if33.pdf (accessed on 24 May 2021).
181. Hummel, S.; Hudak, A.T.; Uebler, E.H.; Falkowski, M.J.; Megown, K.A. A Comparison of Accuracy and Cost of LiDAR versus Stand Exam Data for Landscape Management on the Malheur National Forest. *J. For.* **2011**, *109*, 267–273. [CrossRef]
182. LAND INFO Worldwide Mapping, L. Satellite Imagery Pricing—Satellite Imagery Solutions & Digital Map Data—LAND INFO Worldwide Mapping. Available online: https://landinfo.com/satellite-imagery-pricing/ (accessed on 18 May 2021).
183. Green Structure and Urban Planning—Final Report. Available online: https://www.cost.eu/publications/green-structure-and-urban-planning-final-report/ (accessed on 17 August 2020).
184. Sturiale, L.; Scuderi, A. The Role of Green Infrastructures in Urban Planning for Climate Change Adaptation. *Climate* **2019**, *7*, 119. [CrossRef]